IEEE Open Journal of Signal Processing

Received 5 May 2022; revised 20 July 2022; accepted 24 July 2022. Date of publication 27 July 2022;
date of current version 9 August 2022. The review of this article was arranged by Associate Editor Christos Masouros.

Digital Object Identifier 10.1109/OJSP.2022.3194416

A Downlink RIS-Aided NOMA System With Hardware Impairments: Performance Characterization and Analysis

MOHD HAMZA NAIM SHAIKH [1], VIVEK ASHOK BOHARA [1] (Senior Member, IEEE), ANAND SRIVASTAVA [1], AND GOURAB GHATAK [2]

[1]Wirocomm Research Group, IIIT-Delhi, Delhi 110020, India
[2]Department of Electrical Engineering, IIT-Delhi, Delhi 110016, India

CORRESPONDING AUTHOR: MOHD HAMZA NAIM SHAIKH (e-mail: hamzan@iiitd.ac.in)

ABSTRACT Reconfigurable intelligent surface (RIS) has recently been envisioned to provide an adaptable channel for futuristic wireless communication networks. This work characterized the impact of hardware impairments in the downlink RIS-aided non-orthogonal multiple access (NOMA) wireless networks. We considered the hardware impairments in the transceivers of the base station (BS) and users, phase error at the RIS and the imperfect successive interference cancellation (SIC) for the NOMA users. Specifically, the performance is evaluated by deriving the closed-form expressions for the outage probability (OP), spectral efficiency (SE) and energy efficiency (EE). Additionally, the performance of the orthogonal multiple access (OMA) system is also evaluated and compared with its NOMA counterpart. The RIS-aided NOMA outperforms OMA for the ideal hardware scenario. However, the hardware impairments significantly deteriorate RIS-aided NOMA's performance compared to RIS-aided OMA. Further, we have also compared the proposed RIS-aided NOMA with the baseline full-duplex relaying (FDR) based NOMA. The results show that the gains are more significant for a RIS-aided system than FDR.

INDEX TERMS Reconfigurable intelligent surfaces, sixth-generation, non-orthogonal multiple access, full-duplex relaying, performance analysis, outage probability, spectral efficiency, energy efficiency, decode-and-forward, hardware impairments.

I. INTRODUCTION

For the futuristic wireless network, the research community has started looking towards developing the next generation (presumably, 6 G) for 2030 and beyond [1]. As per the initial findings reported in [2], high-fidelity mobile hologram, digital twin and extended reality (XR) are the three new verticals that will dominate the 6 G services. A few of the requirements to support these innovations are ultra-high peak data rate touching up to 1000 Gbps and user-experienced data rate of up to 1 Gbps with an end-to-end delay of less than 0.1 ms [3]–[5]. Several promising techniques have emerged recently, having strong potential to enhance the performance of beyond 5 G (B5G) wireless networks. Some of them are cell-free massive multiple-input multiple-output (MIMO) systems [6], wireless energy harvesting (W-EH) [7], unmanned aerial vehicles (UAV) communications [8], full-duplex (FD) communication [9], optical wireless communication (OWC) systems [10], and Terahertz (THz) communications [11]. In addition to the above, recently, the concept of reconfigurable intelligent surfaces (RISs) has been widely studied due to its potential to transform the unknown wireless channel into a pervasive network. With this potential, RISs have recently emerged as a revolutionary technology for the 6 G wireless networks [12].

RIS is an array of a large number of reflecting elements (REs) independently capable of altering the reflected signal with the required phase shift. Consequently, through suitable adjustment of the phase, RIS establishes a favorable channel response and thus, offers an additional degree of freedom for enhancing the capacity and increasing the coverage. Further, in addition to improving the received signal strength at the desired destination, RIS can also steer the reflected

beam away from an eavesdropper, thus, providing a secure transmission [13]. Intelligent reflecting surfaces (IRSs) and large intelligent surfaces (LISs) are also commonly referred terminologies for RISs and are used interchangeably in literature [14]. With a large number of passive REs, the RISs are known to have a very large spectral efficiency (SE) as well as energy efficiency (EE) [15]. The easier installation of the RIS structure facilitates a broader deployment across the various urban infrastructure in indoor and outdoor environments, like the home ceilings, factories, roof-tops, street lights, and traffic signal poles. Consequently, RIS can be integrated easily within the existing wireless communication networks [16].

In addition to the above, the multitude of wireless access demands has led to looking beyond the conventional multiple access techniques where the users are multiplexed orthogonally either in time, frequency or through codes. The multiplexing in time is known as time division multiple access (TDMA), the multiplexing in frequency is termed as frequency division multiple access (FDMA), and the multiplexing in code is known as code division multiple access (CDMA). Consequently, the novel concept of non-orthogonal multiple access (NOMA) was explored in developing 5 G wireless standards. NOMA is a promising multiple access technique that can improve SE and user fairness by serving multiple users within the same time-frequency resource block. The multiplexing of users can be done via a power domain or code domain. Specifically, in the power domain NOMA, the users are served simultaneously through a superimposed signal with power coding. While at the user end, the user can decode its own information signal by considering the messages of other users as a perturbation noise. The successive interference cancellation (SIC) technique is adopted at the receiver to decode the superimposed signals in the power domain [17]. With these advantages, NOMA provides better SE and user fairness in multiuser communication compared to the orthogonal multiple access (OMA) [18].

A. RELATED WORK

1) RIS-AIDED NETWORKS

Asymptotic sum rate and outage for the uplink of RIS-assisted system with a Rician distributed channel has been evaluated in [14]. RIS is adopted for enhancing the EE of a downlink multiuser communication scenario in [19]. Likewise, in [20], RIS is employed for enhancing energy harvesting in a simultaneous wireless information and power transfer (SWIPT) system. Further in [21], a self-sustainable RIS has been proposed that harvests energy for the wireless powered communication network (WPCN). The presence of RIS improves the downlink energy transfer and thus enhances the energy harvested by the users, which is utilized for uplink information transmission from these multiple users. RIS has also been employed for vehicular communication in [22], where RIS enhances the performance of both the links, viz. vehicle-to-vehicle (V2V) and vehicle-to-infrastructure (V2I). Further, in [23], RIS has been explored for physical layer security (PLS).

Additionally, the performance of RIS-assisted systems has been evaluated under transceiver hardware impairments in [24]–[26]. However, the effect of phase error was not investigated. In contrast, the authors have investigated the impact of phase error on the performance of RIS-enabled systems under the assumptions of ideal transceiver hardware in [27]–[29]. Furthermore, a novel and practical phase shift model that captures the coupled nature of amplitude and phase for the REs has been proposed in [30], where the authors have evaluated the performance gain that can be achieved by considering the practical phase shift model for beamforming optimizing. Bjornson et al. have compared the performance of RIS-aided systems against decode-and-forward (DF) relaying aided systems. The authors have shown that for many REs, the RIS can easily outperform DF relaying [31]. A comprehensive discussion of the state-of-art research can be found in [32], where Renzo et al. have presented an electromagnetic theory-based communication framework for modeling, analysis, optimization and deployment of a futuristic RIS-empowered smart radio environment. Additionally, [33]–[35] provides a comprehensive review for RIS empowered smart radio communication.

2) RIS-AIDED NOMA NETWORKS

As both RIS and NOMA are highly promising techniques, RIS has been integrated with NOMA in [36]. It has been shown that the combination of RIS and NOMA supports high data rate transmission with improved system performance. Additionally, RIS-aided NOMA provides better utilization of spectral resources. A simple design for downlink transmission of RIS-assisted NOMA has been proposed in [37], where the RIS is deployed to effectively serve the cell-edge user by aligning the reflected beam from RIS. An energy-efficient algorithm for RIS-assisted NOMA has been proposed in [38], where the authors have discussed the tradeoff between the sum rate of NOMA users and total power consumption. In [39] and [40], the performance of the RIS-assisted NOMA is evaluated and compared with OMA. Further, the authors have also proved that the RIS-assisted NOMA performs better than the RIS-assisted OMA. The beamforming vector is optimized to minimize the transmit power in RIS-assisted NOMA systems in [41], while a joint optimization of active beamforming at BS and passive beamforming at RIS to maximize the user sum rate is studied in [42]. Furthermore, in [43], the authors have investigated the resource allocation problem for a downlink RIS NOMA system, where they have proposed a three-step resource allocation algorithm for joint optimization of decoding order of NOMA users, power allocation and reflection coefficients at RIS. Finally, a signal cancellation-based design is employed to simultaneously serve a pair of NOMA users in a MIMO-IRS network [44]. A summary of the related work is also presented in the tabular form in Table I.

As evident from above, RIS-aided NOMA systems have been investigated in the literature. However, these prior studies consider ideal hardware, overlooking the impact of

TABLE I Related Work

Reference	Work	Contribution	Major Difference
Sena *et al*. [36]	Role of IRS in MIMO-NOMA	Discuss different design aspects, challenges and future research direction for IRS-NOMA networks	Ideal Transceiver
Ding & Poor [37]	Simple IRS-NOMA Design	Analyzed the outage probability of IRS-NOMA with and without hardware impairment	Ideal Transceiver
Fang *et al*. [38]	Energy-efficient IRS-NOMA design	Tradeoff between maximizing the sum-rate and minimizing the total power consumption	Ideal Transceiver
Hou *et al*. [39]	Performance analysis of RIS-Aided NOMA	Analytical performance of RIS-NOMA network in terms of SE, EE and outage probability	Ideal Transceiver
Cheng *et al*. [40]	Performance analysis of IRS aided NOMA & OMA	Outage probability and ergodic rate for uplink & downlink of IRS-NOMA and OMA network	Ideal Transceiver
Zhu *et al*. [41]	Power-efficient IRS-assisted MISO NOMA system	Optimized beamforming vectors at BS and phase shift matrix at IRS for minimizing transmit power at the BS	Ideal Transceiver
Mu *et al*. [42]	Joint beamforming IRS-aided MISO NOMA	Maximized the user sum-rate through jointly optimizing the active beamforming at BS and passive beamforming at IRS	Ideal Transceiver
Zuo *et al*. [43]	Resource allocation IRS-NOMA	Joint optimization of the decoding order of NOMA users, power allocation and reflection coefficients at the IRS	Ideal Transceiver
Hou *et al*. [44]	Signal canceling based design of IRS-NOMA	Passive beamforming weights at RIS to serve the paired users simultaneously in a MIMO-NOMA network	Ideal Transceiver
Hemath *et al*. [45]	Hardware Impaired IRS-NOMA	Analysis of outage performance of the IRS-NOMA in the presence of hardware impairments	Non-Ideal Transceiver, Outage Analysis for the specific case of Rayleigh fading

hardware impairments. Further, it has been shown in [45] that the presence of non-ideal hardware severely restricts the performance of a RIS-assisted wireless communication system. Consequently, the gain reported in the SE, EE of RIS-assisted NOMA system in the previous studies needs to be re-examined considering the impact of hardware impairments at BS, RIS and user.

B. CONTRIBUTIONS

Motivated by the above, in this work, we analyze the performance of a RIS-aided NOMA system in the presence of non-ideal hardware at BS and phase error at the RIS. We have also considered the impact of imperfect SIC on the NOMA user pair. The main contributions of the proposed work are summarized below.

- We investigate the performance of the RIS-aided NOMA system in the presence of hardware impairments at BS, RIS and users. The proposed analysis considers the impact of channel fading, the size of RIS in terms of the number of REs, the severity of hardware impairment and the imperfect SIC.
- Explicitly, we derive the closed-form expressions for the outage probability (OP), SE and the EE of the proposed RIS-aided NOMA network by initially formulating the signal-to-distortion-plus-interference-plus-noise-ratio (SDINR) and then utilizing it to derive the above expressions for both the near and far user.
- Further, we demonstrate that although the number of REs, transmit power and Rician factor affect the performance in the low SNR region. However, they do not influence the high-SNR region. The level of hardware impairment solely limits the high-SNR performance. Beyond the saturation region, there is no impact of increasing the number of REs or transmit power.
- Finally, as a performance benchmark, the obtained results of the proposed work are compared with an ideal RIS-aided NOMA and OMA system. The results show that irrespective of the level of distortion, the NOMA scenario outperforms the OMA for both ideal and non-ideal hardware cases. Additionally, the performance is also compared with full-duplex relaying (FDR). The results show significant performance gain can be realized by employing RIS over FDR.

So as compared to [45], where the investigation was restricted only to outage analysis without considering the SE and the EE, this work comprises a complete analytical framework to analyze the SE and EE performance of a RIS-aided NOMA system under the nonlinear transceiver at BS and users as well as phase error at the RIS. Moreover, the authors in [45] have also restricted to the specific case of the Rayleigh fading scenario, which may not be a practical use case scenario since RISs are usually deployed to have a line-of-sight (LoS) with the base station (BS) or the users. In contrast, this work considers a more realistic Rician fading model to model the LoS link characteristics. Furthermore, the efficacy of the analytical derivations has also been validated through simulations.

C. ORGANIZATION AND NOTATIONS

The remaining paper is organized as follows: Section II discusses the details of the system model for the RIS-aided NOMA network. Section III presents the received signal

TABLE II Notations

Symbol	Definition
$\mathbb{E}[\cdot]$	Expectation Operator
$\mathbb{P}[\cdot]$	Probability
$\mathrm{tr}[\cdot]$	Trace Operator
$[\cdot]^{\mathrm{H}}$	Hermitian Operator
$\mathrm{E}_i(\cdot)$	Exponential Integral
$\Gamma(\cdot)$	Gamma Function
$\Psi(\cdot)$	Digamma Function
$\psi^{(v)}(\cdot)$	Polygamma Function of v order
$\gamma(\cdot,\cdot)$	Lower Incomplete Gamma Function
${}_pF_q(\cdot,\cdot;\cdot;\cdot)$	Gauss Hyper-Geometric Function
$I_v(.)$	Modified Bessel Function (first kind & order v)
$f_{\mathcal{G}}(x)$, $F_{\mathcal{G}}(x)$	PDF and CDF of RV $\mathcal{G}$

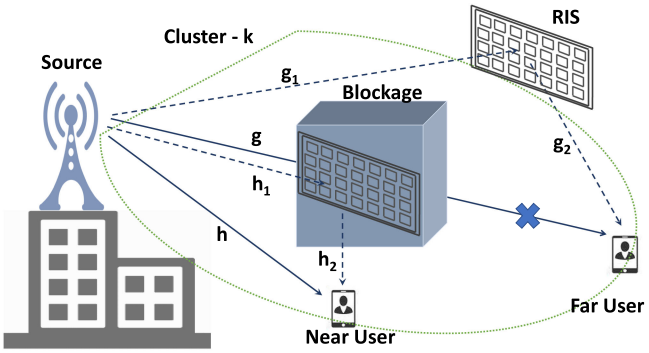

FIGURE 1. Schematic for the considered downlink RIS-aided NOMA wireless system.

model, while Section IV analyzes the performance of the proposed system. Simulation results are presented in Section V, and finally, Section VI concludes the paper.

The major notations used are been summarized here: Boldface lower case represent vectors (e.g., $\mathbf{x}$) and upper cases represents matrices (e.g., $\mathbf{X}$). $\mathcal{CN}(\mu, \sigma^2)$ denotes a complex Gaussian distribution with mean, μ, and variance σ^2. In addition, Table II summarizes the remaining notations.

II. SYSTEM MODEL

We consider a downlink communication scenario where a single antenna BS communicates with multiple users. The multiple users are grouped into clusters, and each cluster can be supported through an orthogonal resource block. Since all the clusters are identical, subsequently, we will restrict our analysis to one such representative cluster[1]. As illustrated in Fig. 1, within each cluster, the near user (NU) is assumed to be around the center of the cell. In contrast, the far user (FU) is assumed to be at the cell edge. Both the users are supported through NOMA protocol[2]. In line with the assumptions of earlier work, [40], the FU cannot communicate with the BS due to more significant distance and blockages, whereas the BS can communicate with the NU [37]. In order to enhance the performance of NU, a RIS is also employed, which consists of M number of REs (here, $M > 1$). Further, as the direct link between the BS and FU is blocked, another RIS is employed to assist the transmission between the FU and BS through the reflected link (here also, the RIS consists of M number of REs).

A. CHANNEL MODEL

The channel is assumed to be quasi-static and flat fading. It is also assumed that the channel state information (CSI) is perfectly known[3] at the BS, similar to the prior works of [37], [41]. Since the RISs are deployed to have an LoS link with the BS and the UEs, the small-scale fading coefficients for the BS-to-RIS, RIS-to-NU and RIS-to-FU links, $\mathbf{h}_1$, $\mathbf{h}_2$, $\mathbf{g}_1$ and $\mathbf{g}_2$ can be characterized through the Rician fading model [51]. In contrast, there is no LoS link between the BS-to-NU. Hence, h can be characterized through the Rayleigh fading model, thus, $h \sim \mathcal{CN}(0, 1)$ [52].

B. HARDWARE IMPAIRMENTS

This subsection describes the transceiver's non-idealities that result in the distortion of the actual received signal from the desired transmitted signal. Specifically, in the proposed downlink RIS-aided NOMA system, the hardware impairment exists in the transceiver at BS. In addition, a phase error also occurs due to the presence of non-ideal hardware at the RIS.

1) TRANSCEIVER IMPAIRMENTS

It has been shown in the literature that the assumption of ideal hardware while evaluating the performance of wireless communication systems is not practical. This is because of the fact that the transceiver architecture at the RF front-end is prone to several inevitable additive impairments like the in-phase/quadrature (I/Q) imbalance, the nonlinearity of the radio front-end and the phase noise at the oscillator. Fig. 2 illustrates the block diagram of a typical transmitter. The schematic shows that the baseband I and Q signals are up-converted after passing through the modulator to the required RF. Further, an ideal local oscillator (LO) is deployed to achieve a precise 90-degree phase shift between the I/Q branches while maintaining equal gain. However, because of the non-idealities in the LO circuitry, the realized phase shift is not exactly 90 degrees resulting into phase imbalance. This causes a gain mismatch. The joint impact of gain imbalance and phase mismatch is called I/Q imbalance. Likewise, the power amplifier (PA), which is usually the last component

[1] Although the results are derived for a single antenna BS, they can easily be extended for a MIMO-NOMA network, where precoding can decompose the MIMO-NOMA to multiple separate SISO-NOMA [40]. Thus, the inter-cluster interference can be suppressed through precoding while SIC mitigates the intra-cluster interference [18].

[2] There can be multiple users within the cluster, however, due to complexity requirements, we are restricting ourselves to a 2-user case, similar to [46], [47].

[3] Several channel estimations techniques are proposed in the literature for RIS-assisted networks, in particular, [48]–[50] are known to provide an accurate estimation of CSI at BS.

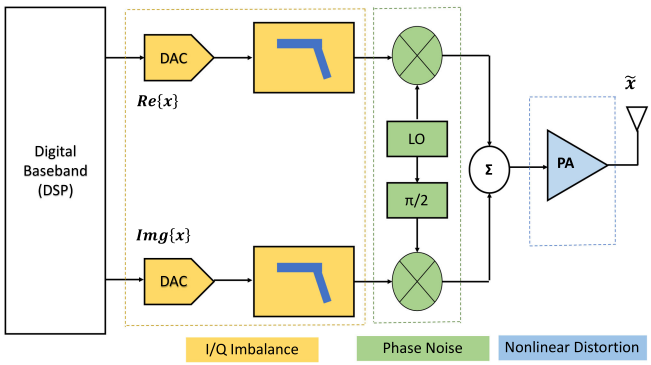

FIGURE 2. Schematic showing various imperfections at the source transceiver.

in the transmit chain, is a nonlinear device that causes both in-band and out-of-band distortion. As a result, the error vector magnitude (EVM) degrades. Further, it also results in the spectral regrowth of the transmitted signal.

These residual impairments result into distortion, which can be characterized as a) multiplicative, in which the received signals are phase-shifted; b) additive, in which a distortion noise is added whose variance is proportional to the power of the transmitted and received signals; and c) amplified thermal noise [53]. A generic approach for modeling the collective impact of all these impairments considers that the resultant 'distortion' noise is Gaussian distributed, with the average power being proportional to the average transmit power of the signal. Moreover, it can also be noted here that this Gaussian characterization has been experimentally validated as discussed in literature [54].

Hence, the above imperfections at the source will result in a mismatch between the actual signal, x, where $x \in \mathcal{CN}(0, \sigma_{in}^2)$, and the signal transmitted by the non-ideal transceiver, $\tilde{x}$, which can be expressed as

$$\tilde{x} = x + w, \tag{1}$$

where w represents the aggregated distortion noise that is caused by the various hardware imperfections. It can be modeled as a zero-mean complex Gaussian random variable (RV) whose variance can be expressed as

$$\sigma_w^2 = \zeta^2 \sigma_{in}^2, \tag{2}$$

where ζ is a proportionality constant that characterize the level of residual impairment at the source.

2) RIS IMPAIRMENTS

Ideally, the RIS is configured to provide a phase shift that cancels the overall phase shift and thus maximizes the received signal power at the desired receiver. However, a residual phase error exists in the actual phase shift imparted by the RIS, which occurs due to these two possible reasons. This deviation of the actual phase shift from the ideally desired phase shift is modeled by setting the phase noise Θ, a random variable in $[-\pi, \pi)$.

- The first reason for the residual phase error is the imperfect channel estimate at the RIS and termed as the phase estimation error. Specifically, for this scenario, Θ is modeled as a zero-mean von Mises variable. Here, τ is the concentration parameter that captures the channel estimation accuracy. Further, in this case, the characteristic function is $\varphi_p = \frac{I_p(\tau)}{I_0(\tau)}$ [29].
- Likewise, the second reason is the hardware imperfection due to practical hardware at the RIS. Here only a set of discrete phase shifts, 2^q $(q \geq 1)$, are available instead of the ideally infinite phase shifts. Moreover, the error Θ is assumed to be uniformly distributed over $[-2^{-q}\pi, 2^{-q}\pi]$ [55]. For this case, the characteristic function can be defined as $\varphi_1 = \frac{\sin(2^{-q}\pi)}{2^{-q}\pi}$ and $\varphi_2 = \frac{\sin(2^{-q+1}\pi)}{2^{-q+1}\pi}$ [29].

C. NOMA PROTOCOL

Now the superimposed signal for both the user that will be transmitted from the BS to the paired NOMA user is:

$$x = \beta_n x_n + \beta_f x_f, \tag{3}$$

where x_n and x_f denote the desired signal of NU and FU, respectively. The power allocation coefficients, β_n and β_f, for NU and FU, respectively follows the NOMA constraint $\beta_n^2 + \beta_f^2 = 1$. For the sake of user fairness between the NOMA pair, we use $\beta_n < \beta_f$.

Since the transmitted signal is impaired by the non-ideal hardware and thus, from (1), the transmitted signal from the BS can be written as

$$\tilde{x} = \beta_n x_n + \beta_f x_f + w_s, \tag{4}$$

where $w_s \in \mathcal{CN}(0, \kappa_s^2 P_s)$ is the distortion noise due to hardware impairments at BS, and P_s denotes the transmit power at the BS.

D. PATHLOSS MODELING

A 3GPP Urban Micro (UMi) pathloss model, as described and discussed in [31], characterizes the large-scale fading. So, at the carrier frequency of 3 GHz, the pathloss $\mathcal{B}$ at a distance of d meter can be expressed as:

$$\mathcal{B}(d)\ [\text{dB}] = G_{\text{t}}\ [\text{dBi}] + G_{\text{r}}\ [\text{dBi}] + \begin{cases} -37.5 - 22\log_{10}(d/1\,\text{m}) & \text{if LoS}, \\ -35.1 - 36.7\log_{10}(d/1\,\text{m}) & \text{if NLoS}, \end{cases} \tag{5}$$

where G_{t} and G_{r} denote the transmit and receive antenna gain at the source/relay and relay/destination, respectively.

III. RECEIVED SIGNAL MODEL AND SNR FORMULATION

This section evaluates the SNR formulation for the NU and FU. Initially, the received signal model is described, and then RIS parameters are optimized to give the maximum SNR.

A. NEAR USER

1) RECEIVED SIGNAL AT NU

The received signal at the NU comprises of the direct link as well as the reflected link via RIS. Thus the received signal at NU, y_n, can be expressed as

$$y_n = \left[\sqrt{\mathcal{B}_h}\, h + \sqrt{\mathcal{B}_{h_1}\mathcal{B}_{h_2}}\mathbf{h}_1\, \mathbf{\Phi}\, \mathbf{h}_2\right] \times \left(\beta_n\, x_n + \beta_f\, x_f + w_s\right)\, \sqrt{P_s} + w_{d_1} + N_o, \quad (6)$$

where $\mathcal{B}_h$ is the pathloss for the direct path between BS and NU, while $\mathcal{B}_{h_1}$, $\mathcal{B}_{h_2}$ are the pathloss for the reflected link, i.e., BS-to-RIS and RIS-to-NU, respectively. Further, $\mathbf{\Phi}$ is the reflection coefficient matrix of the RIS and $w_{d_1} \in \mathcal{CN}(0, \kappa_{d_1}^2\ |\sqrt{\mathcal{B}_h}\, h + \sqrt{\mathcal{B}_{h_1}\ \mathcal{B}_{h_2}}\, \mathbf{h}_1 \mathbf{\Phi} \mathbf{h}_2|^2 P_s)$ represents the aggregated distortion noise due to the non-ideal transceiver at the NU. Also, $h = |h|e^{-j\phi}$ is the small scale fading co-efficient for the direct link between the BS and the NU, where $|h|$ is the channel amplitude characterized through the Rayleigh RV and ϕ is the channel phase. Finally, N_o is the additive white Gaussian noise (AWGN) with $N_o \in \mathcal{CN}(0, \sigma^2)$.

On expanding (6), we can re-write the received signal at NU as

$$y_n = \left[\sqrt{\mathcal{B}_h}\, h + \sqrt{\mathcal{B}_{h_1}\mathcal{B}_{h_2}} \sum_{i=1}^{M} h_1^i\ \Phi^i\ h_2^i\right] \times \left(\beta_n\, x_n + \beta_f\, x_f + w_s\right) \sqrt{P_s} + w_{d_1} + N_o, \quad (7)$$

where, $h_1^i = |h_1^i|e^{-j\phi_1^i}$ is the channel co-efficient between the BS to the i-th reflecting element of RIS with amplitude, $|h_1^i|$, and phase, ϕ_1^i. Similarly, $h_2^i = |h_2^i|e^{-j\phi_2^i}$ is the channel coefficient between the i-th reflecting element of the RIS to NU with amplitude, $|h_2^i|$, and phase, ϕ_2^i. The envelopes of h_1^i and h_2^i for $i = 1, \ldots, M$ are i.i.d and characterized through Rician RV with a shape and scale factor of K_1, K_2 and Ω_1, Ω_2, respectively. It is also assumed that $\mathbf{h}_1$ and $\mathbf{h}_2$ are mutually independent of h and of each other.

2) RIS REFLECTION PARAMETERS

Now by optimizing the reflection matrix, $\mathbf{\Phi}$, the total channel gain for the NU can be maximized, i.e., $|\sqrt{\mathcal{B}_h}\, h + \sqrt{\mathcal{B}_{h_1}\mathcal{B}_{h_2}}\, \mathbf{h}_1 \mathbf{\Phi} \mathbf{h}_2|$. This can be achieved by adjusting θ^i to cancel the resultant phase of h_1^i, h_2^i and h. Thus, by applying $\theta^i = \phi - \phi_1^i + \phi_2^i$, the channel gain will be maximized and can be expressed as

$$|\mathcal{H}|^2 = \left|\sqrt{\mathcal{B}_h}\, h + \sqrt{\mathcal{B}_{h_1}\mathcal{B}_{h_2}}\, \mathbf{h}_1 \mathbf{\Phi} \mathbf{h}_2\right|^2, = \left(\sqrt{\mathcal{B}_h}\ |h| + \sqrt{\mathcal{B}_{h_1}\mathcal{B}_{h_2}} \sum_{i=1}^{M} \left|h_1^i\right| \left|h_2^i\right|\right)^2. \quad (8)$$

However, due to the presence of non-ideal hardware at the RIS, θ^i may not be able to cancel the resultant phase of h_1^i, h_2^i and h. Thus, the resultant channel gain will comprises of the phase error which can be expressed as

$$|\mathcal{H}|^2 = \left(\sqrt{\mathcal{B}_h}\ |h| + \sqrt{\mathcal{B}_{h_1}\mathcal{B}_{h_2}} \sum_{i=1}^{M} \left|h_1^i\right| \left|h_2^i\right|\ e^{j\Theta_i}\right)^2, \quad (9)$$

or equivalently

$$|\mathcal{H}|^2 = \left(\sqrt{\mathcal{B}_h}\ |h| + \sqrt{\mathcal{B}_{h_1}\mathcal{B}_{h_2}}\, M\ |H|\right)^2, \quad (10)$$

where $H = \frac{1}{M}\sum_{i=1}^{M} |h_1^i||h_2^i|\, e^{j\Theta_i}$.

Utilizing (10), the received signal at NU in (7) can now be expressed as

$$y_n = |\mathcal{H}|^2 \left(\beta_n\, x_n + \beta_f\, x_f\right)\, \sqrt{P_s} + w_1 + N_o, \quad (11)$$

where

$$w_1 = |\mathcal{H}|^2\, w_s + w_{d_1}, \quad (12)$$

denotes the aggregated distortion caused by the transceiver impairments at the BS and NU.

3) SNR FORMULATION

At NU, initially, the NU will decode the signal of FU with the following signal-to-distortion-plus-interference-plus-noise ratio (SDINR).

$$SDINR_{n\to f} = \frac{|\mathcal{H}|^2\, \beta_f^2\, P_s}{|\mathcal{H}|^2\, \beta_n^2\, P_s + |\mathcal{H}|^2 \left(\kappa_s^2 + \kappa_{d_1}^2\right) P_s + \sigma^2}. \quad (13)$$

After decoding and canceling the signal of FU, the NU can decode its own signal. However, due to the presence of non-idealities, NU may not be able to implement perfect SIC. Hence due to imperfect SIC, the NU will experience a residual interference of the FU signal. Based on imperfect SIC, the SDINR at NU can be expressed as

$$SDINR_n = \frac{|\mathcal{H}|^2\, \beta_n^2\, P_s}{\xi\ |\mathcal{H}|^2\, \beta_f^2\, P_s + |\mathcal{H}|^2 \left(\kappa_s^2 + \kappa_{d_1}^2\right) P_s + \sigma^2}, \quad (14)$$

where $\xi \in [0, 1]$ represents the error propagation model that captures the efficacy of SIC. Specifically, $\xi = 0$ corresponds to the ideal scenario of perfect SIC while $\xi = 1$ corresponds to scenario of maximum interference [56].

After rearranging the terms of 14, the SDINR at NU can be expressed as

$$SDINR_n = \frac{|\mathcal{H}|^2\, \beta_n^2\, \Upsilon_s}{|\mathcal{H}|^2 \left(\xi\ \beta_f^2 + \kappa_s^2 + \kappa_{d_1}^2\right) \Upsilon_s + 1}, \quad (15)$$

where $\Upsilon_s = \frac{P_s}{\sigma^2}$ is the transmit signal-to-noise ratio (SNR).

Thus, the normalized instantaneous rate for the NU, R_n, can be evaluated from the SDINR at the NU as

$$R_n = \log_2\left(1 + SDINR_n\right), = \log_2\left(1 + \frac{|\mathcal{H}|^2\, \beta_n^2\, \Upsilon_s}{|\mathcal{H}|^2 \left(\xi\ \beta_f^2 + \kappa_s^2 + \kappa_{d_1}^2\right) \Upsilon_s + 1}\right). \quad (16)$$

B. FAR USER

1) RECEIVED SIGNAL AT FU

As discussed in system model, the RIS is employed to assist the BS-FU communication through the reflected link, i.e., BS-RIS-FU link. Thus, the received signal at FU, y_f, can be expressed as

$$y_f = \sqrt{\mathcal{B}_{g_1}\mathcal{B}_{g_2}}\,\mathbf{g}_1\,\mathbf{\Phi}\,\mathbf{g}_2\,\left(\beta_n x_n + \beta_f x_f + w_s\right)\sqrt{P_s} + w_{d_2} + N_o, \quad (17)$$

where $\mathcal{B}_{g_1}$, $\mathcal{B}_{g_2}$ represents the pathloss of the BS-to-RIS and RIS-to-FU link, respectively and $w_{d_2} \in \mathcal{CN}(0, \kappa_{d_2}^2\,|\mathbf{g}_1\mathbf{\Phi}\mathbf{g}_2|^2\mathcal{B}_{g_1}\mathcal{B}_{g_2}P_s)$ represents the aggregated distortion noise due to the non-ideal transceiver at the FU. Further, $\mathbf{\Phi}$ is the reflection coefficient matrix of the RIS, where $\mathbf{\Phi} = \text{diag}(\Phi_i)$ and Φ_i is the response of i-th RE. Now, $\Phi_i = \delta_i\phi_i$ with $\delta_i \in (0, 1]$, being the amplitude reflection coefficient and $\phi_i = e^{j\theta_i}$ being the phase shift introduced by the i-th RE, where $j = \sqrt{-1}$ and $\theta \in [0, 2\pi)\ \forall\, i = 1, \ldots, M$.

On further expanding (17), we can have

$$y_f = \sqrt{\mathcal{B}_{g_1}\mathcal{B}_{g_2}}\left[\sum_{i=1}^{M} g_1^i\,\Phi^i\,g_2^i\right]\left(\beta_n x_n + \beta_f x_f + w_s\right)\sqrt{P_s} + w_{d_2} + N_o, \quad (18)$$

where $g_1^i = |g_1^i|e^{-j\varpi_1^i}$ is the channel co-efficient between the BS to the i-th reflecting element of RIS with $|g_1^i|$ being the amplitude and ϖ_1^i being the phase shift. Similarly, $g_2^i = |g_2^i|e^{-j\varpi_2^i}$ is the channel coefficient between the i-th reflecting element of the RIS to FU with $|g_2^i|$ and ϖ_2^i being the channel amplitude and phase, respectively. Moreover, the envelopes of g_1^i for $i = 1, \ldots, M$ are assumed to be independent and identically distributed (i.i.d) and characterized by the Rician RV with a shape and scale factor of K_3 and Ω_3, respectively. Similarly for g_2, the elements are also i.i.d and Rician distributed with a shape and scale parameter of K_4 and Ω_4, respectively. Additionally, it is also assumed that $\mathbf{g}_1$ and $\mathbf{g}_2$ are independent of each other.

2) RIS REFLECTION PARAMETERS

Now by optimizing the reflection matrix, $\mathbf{\Phi}$, the channel gain can be maximized, i.e., $|\mathbf{g}_1\mathbf{\Phi}\mathbf{g}_2|$. This can be achieved by adjusting θ^i to cancel the resultant phase of g_1^i and g_2^i. Thus, by applying $\theta^i = \varpi_1^i + \varpi_2^i$, $|\mathbf{g}_1\mathbf{\Phi}\mathbf{g}_2|$ can be maximized and this optimal solution can be denoted as $\tilde{\theta}$. Thus, the maximum channel gain can be expressed as

$$|\mathcal{G}|^2 = \mathcal{B}_{g_1}\mathcal{B}_{g_2}\,|\mathbf{g}_1\mathbf{\Phi}\mathbf{g}_2|^2, = \mathcal{B}_{g_1}\mathcal{B}_{g_2}\left(\sum_{i=1}^{M}\left|g_1^i\right|\left|g_2^i\right|\right)^2, \quad (19)$$

where it is assumed that $\delta^i = 1, \forall\, i$, without any loss of generality. Further, as the RIS is also impaired by the unavailability of ideal phase shift, $\tilde{\theta}$, in practice the maximum channel gain that can be achieved can be expressed as

$$|\mathcal{G}|^2 = \mathcal{B}_{g_1}\mathcal{B}_{g_2}\left(\sum_{i=1}^{M}\left|g_1^i\right|\left|g_2^i\right|\exp\left(j\Theta_i\right)\right)^2, \quad (20)$$

or equivalently,

$$|\mathcal{G}|^2 = M^2\,\mathcal{B}_{g_1}\mathcal{B}_{g_2}\,|G|^2, \quad (21)$$

where $G = \frac{1}{M}\sum_{i=1}^{M}|g_1^i||g_2^i|\exp\left(j\Theta_i\right)$.

Hence, from (21), the received signal at FU in (18) can be re-written as

$$y_f = |\mathcal{G}|^2\left(\beta_n x_n + \beta_f x_f + w_s\right)\sqrt{P_s} + w_{d_2} + N_o, \quad (22)$$

which on simplification gives

$$y_f = |\mathcal{G}|^2\left(\beta_n x_n + \beta_f x_f\right)\sqrt{P_s} + w_2 + N_o, \quad (23)$$

where

$$w_2 = |\mathcal{G}|^2\,w_s + w_{d_2}, \quad (24)$$

is the aggregated distortion caused by the transceiver impairments at the BS and FU.

Thus, for a given channel realization, w_1 and w_2 in (11) and (23), can be characterized as zero mean noise with variance [24]

$$\sigma_{w1}^2 = |\mathcal{H}|^2\left(\kappa_s^2 + \kappa_{d_1}^2\right)P_s,$$
$$\sigma_{w2}^2 = |\mathcal{G}|^2\left(\kappa_s^2 + \kappa_{d_2}^2\right)P_s. \quad (25)$$

Here, κ_s, κ_{d_1} and κ_{d_2} are the proportionality constant that controls the level of impairment of the non-ideal transceiver at the BS, NU and FU, respectively. Additionally, it can also be noted here that for $\kappa_s = \kappa_{d_1} = \kappa_{d_2} = 0$, the scenario reduces to the case of ideal transceiver with no distortion, i.e., $w_1 = w_2 = 0$ in both (11) and (23). The performance of the ideal transceiver based NOMA has been studied in [40]. Further from (25), it can also be observed that the distortion noise variance (due to non-ideal transceiver) increases along with signal power.

3) SNR FORMULATION

Likewise, the FU will decode its signal while treating the signal for NU as an interference. Thus, the SDINR at FU can be expressed as

$$SDINR_f = \frac{|\mathcal{G}|^2\,\beta_f^2\,P_s}{|\mathcal{G}|^2\,\beta_n^2\,P_s + |\mathcal{G}|^2\left(\kappa_s^2 + \kappa_{d_2}^2\right)P_s + \sigma^2}. \quad (26)$$

or equivalently

$$SDINR_f = \frac{|\mathcal{G}|^2\,\beta_f^2\,\Upsilon_s}{|\mathcal{G}|^2\left(\beta_n^2 + \kappa_s^2 + \kappa_{d_2}^2\right)\Upsilon_s + 1}. \quad (27)$$

Thus, the normalized instantaneous rate for the FU, R_f, can now be evaluated as

$$R_f = \log_2\left(1 + SDINR_f\right),$$

$$= \log_2\left(1+\frac{|\mathcal{G}|^2\,\beta_f^2\,\Upsilon_s}{|\mathcal{G}|^2\left(\beta_n^2+\kappa_s^2+\kappa_{d_2}^2\right)\Upsilon_s+1}\right). \quad (28)$$

IV. PERFORMANCE ANALYSIS

This section evaluates the performance in terms of the outage, ergodic rates, SE and EE.

A. ERGODIC RATE

The ergodic rate is one of the widely accepted performance metrics used in rate-adaptive systems. The ergodic rate for the NU and FU can be formulated as

$$\bar{R}_n = \mathbb{E}\left[R_n\right], \\ = \mathbb{E}\left[\log_2\left(1+\frac{|\mathcal{H}|^2\,\beta_n^2\,\Upsilon_s}{|\mathcal{H}|^2\left(\xi\,\beta_f^2+\kappa_s^2+\kappa_{d_2}^2\right)\Upsilon_s+1}\right)\right], \quad (29)$$

and

$$\bar{R}_f = \mathbb{E}\left[R_f\right], \\ = \mathbb{E}\left[\log_2\left(1+\frac{|\mathcal{G}|^2\,\beta_f^2\,\Upsilon_s}{|\mathcal{G}|^2\left(\beta_n^2+\kappa_s^2+\kappa_{d_2}^2\right)\Upsilon_s+1}\right)\right], \quad (30)$$

respectively.

Remark 1: The corresponding ergodic rates for the NU and FU can be evaluated by considering the transmission in two equal orthogonal time slots. In each of the slots, the two users are served through TDMA.

Now, the probability distribution function (PDF) of $\mathcal{H}$ is not available in the closed-form. Consequently, the ergodic rate of NU does not admit a closed-form expression. However, it can be approximated tightly by an upper bound [52]. The following Lemma provides an approximate closed form for the upper bound on the ergodic rate of NU and the closed-form expression for the ergodic rate of FU.

Lemma 1: For the considered RIS-aided NOMA system, the ergodic rate of the FU, $\bar{R}_f$, can be expressed as shown in (31) shown at the bottom of this page.

Proof: Please refer to Appendix B for the derivation of $\bar{R}_f$. ■

Remark 2: The ergodic rate for FU, in case of RIS-aided OMA scenario can be extracted from (31) by substituting $\mathcal{C}_1$ and $\mathcal{C}_2$ as $\mathcal{B}M^2\left(1+\kappa_s^2+\kappa_{d_2}^2\right)$ and $\mathcal{B}M^2\left(\kappa_s^2+\kappa_{d_2}^2\right)$, respectively.

Remark 3: The high SNR approximation for the ergodic rate of FU can be given as

$$\bar{R}_f = \log_2\left(1+\frac{\beta_f^2}{\beta_n^2+\kappa_s^2+\kappa_{d_2}^2}\right). \quad (32)$$

This approximation can be derived from (63) by considering the fact that for high SNR (i.e., when Υ is large) $|\mathcal{G}|^2(\kappa_s^2+\kappa_{d_2}^2)\Upsilon_s+1 \approx |\mathcal{G}|^2(\kappa_s^2+\kappa_{d_2}^2)\Upsilon_s$ and thus 1 can be neglected safely. After simplification, the above relationship can easily be found.

Remark 4: Likewise, the high SNR approximation for the ergodic rate of FU for the RIS-aided OMA scenario can be given as

$$\bar{R}_f^O = \log_2\left(1+\frac{1}{\kappa_s^2+\kappa_{d_2}^2}\right). \quad (33)$$

Remark 5: The approximation the ergodic rate of FU for large M can again be given as

$$\bar{R}_f = \left[\log_2\left(1+\frac{\beta_f^2}{\kappa_s^2+\kappa_{d_2}^2+\beta_n^2}\right)\right]. \quad (34)$$

Since the proof is similar to that followed in Remark 3, it is omitted for the sake of brevity.

Remark 6: Likewise, the corresponding approximation of the ergodic rate of FU for large M in the case of RIS-aided OMA can again be given as

$$\bar{R}_f^O = \left[\log_2\left(1+\frac{1}{\kappa_s^2+\kappa_{d_2}^2}\right)\right]. \quad (35)$$

Lemma 2: For the considered RIS-aided NOMA system, the ergodic rate of the NU, $\bar{R}_n$ is upper bounded by $\hat{R}_n$, which can be expressed as shown in (36) shown at bottom of the next page).

Proof: Please refer to Appendix A. ■

Remark 7: Likewise, the upper bound on the ergodic rate of the NU, in case of RIS-aided OMA scenario, can be extracted from (36) by substituting Ξ_1 and Ξ_2 as $(\kappa_s^2+\kappa_{d_1}^2)\Upsilon_s$ and $(\xi\ +\kappa_s^2+\kappa_{d_1}^2)\Upsilon_s$, respectively.

Remark 8: The high SNR approximation for the ergodic rate of NU can be given as

$$\bar{R}_n = \left[\log_2\left(1+\frac{\beta_n^2}{\xi\,\beta_f^2+\kappa_s^2+\kappa_{d_1}^2}\right)\right]. \quad (37)$$

This approximation can be derived from (29) by considering the fact that for high SNR (i.e. when Υ is large) $|\mathcal{H}|^2(\xi\,\beta_f^2+$

$$\bar{R}_f = \frac{m^m}{\Gamma(m)\,\mu^{2\,m}\,\ln(2)}\left[\frac{\pi}{m\,\sin(m\,\pi)}\left\{\frac{{}_1F_1\left(m;\ m+1;\ \frac{m}{\mu^2}\frac{1}{\mathcal{C}_1\,\Upsilon_s}\right)}{(\mathcal{C}_1\,\Upsilon_s)^m}-\frac{{}_1F_1\left(m;\ m+1;\ \frac{m}{\mu^2}\frac{1}{\mathcal{C}_2\,\Upsilon_s}\right)}{(\mathcal{C}_2\,\Upsilon_s)^m}\right\}+\frac{\mu^{2\,m}\,\Gamma(m)}{m^m}\right. \\ \left.\times\left\{\ln\left(\frac{\mathcal{C}_1}{\mathcal{C}_2}\right)+\frac{m}{\mu^2\,(1-m)}\left(\frac{{}_2F_2\left(1,1;\ 2,2-m;\ \frac{m}{\mu^2}\frac{1}{\mathcal{C}_2\,\Upsilon_s}\right)}{\mathcal{C}_2\,\Upsilon_s}-\frac{{}_2F_2\left(1,1;\ 2,2-m;\ \frac{m}{\mu^2}\frac{1}{\mathcal{C}_1\,\Upsilon_s}\right)}{\mathcal{C}_1\,\Upsilon_s}\right)\right\}\right] \quad (31)$$

$\kappa_s^2+\kappa_{d_1}^2)\Upsilon_s+1\approx|\mathcal{H}|^2(\xi\,\beta_f^2+\kappa_s^2+\kappa_{d_1}^2)\Upsilon_s$ and thus 1 can be neglected safely. After simplification, the above relationship can easily be found.

Remark 9: Likewise for the RIS-aided OMA scenario, the high SNR approximation for the ergodic rate of NU can be given as

$$\bar{R}_n^O=\left[\log_2\left(1+\frac{1}{\kappa_s^2+\kappa_{d_1}^2}\right)\right]. \tag{38}$$

Remark 10: The large M approximation for the ergodic rate of NU can again be given as

$$\bar{R}_n=\left[\log_2\left(1+\frac{\beta_n^2}{\xi\,\beta_f^2+\kappa_s^2+\kappa_{d_1}^2}\right)\right]. \tag{39}$$

Since the proof is similar to that followed in Remark 1, it is omitted for the sake of brevity.

Remark 11: Similarly for the RIS-aided OMA scenario, the large M approximation for the ergodic rate of NU can again be given as

$$\bar{R}_n^O=\left[\log_2\left(1+\frac{1}{\kappa_s^2+\kappa_{d_1}^2}\right)\right]. \tag{40}$$

B. OUTAGE PROBABILITY

The outage probability for RIS-aided NOMA system can be defined as probability that instantaneous rate achieved is less than the rate threshold. So, the outage probability at NU can be defined as

$$\begin{aligned}P_n&=\mathbb{P}\left\{R_n<R_{th,n}\right\},\\&=\mathbb{P}\left\{\log_2(1+SDINR_{n\to f})<R_{th,f}\right\}\\&\quad+\mathbb{P}\left\{\log_2(1+SDINR_{n\to f})>R_{th,f}\right\}\\&\quad\times\mathbb{P}\left\{\log_2(1+SDINR_n)<R_{th,n}\right\},\end{aligned} \tag{41}$$

where $R_{th,n}$ and $R_{th,f}$ represent the rate threshold corresponding to the NU and FU, respectively.

Utilizing (41), the OP for the NU can be formulated as

$$\begin{aligned}P_n&=\mathbb{P}\left\{\log_2(1+SDINR_{n\to f})<R_{th,f}\right\}\\&\quad+\mathbb{P}\left\{\log_2(1+SDINR_{n\to f})>R_{th,f}\right\}\\&\quad\times\mathbb{P}\left\{\log_2(1+SDINR_n)<R_{th,n}\right\},X\end{aligned} \tag{42}$$

which can be reformulated as

$$\begin{aligned}P_n=1-&\\&\mathbb{P}\left\{SDINR_{n\to f}\geq 2^{R_{th,f}}-1,SDINR_n\geq 2^{R_{th,n}}-1\right\},\\&=1-\mathbb{P}\left\{SDINR_{n\to f}\geq\chi_f,SDINR_n\geq\chi_n\right\},X\end{aligned} \tag{43}$$

where $\chi_f=2^{R_{th,f}}-1$ and $\chi_n=2^{R_{th,n}}-1$. Utilizing (13) and (14), the outage probability for NU, P_n, can be evaluated as

$$\begin{aligned}P_n=1-\mathbb{P}\Bigg\{&\frac{|\mathcal{H}|^2\,\beta_f^2\,\Upsilon_s}{|\mathcal{H}|^2\left(\beta_n^2+\kappa_s^2+\kappa_{d_1}^2\right)\Upsilon_s+1}\geq\chi_f,\\&\frac{|\mathcal{H}|^2\,\beta_n^2\,\Upsilon_s}{|\mathcal{H}|^2\left(\xi\,\beta_f^2+\kappa_s^2+\kappa_{d_1}^2\right)P_s+1}\geq\chi_n\Bigg\},\end{aligned} \tag{44}$$

which can be simplified as

$$\begin{aligned}P_n=1-\mathbb{P}\Bigg\{&|\mathcal{H}|^2\geq\sqrt{\frac{\chi_f}{\Upsilon_s\left(\beta_f^2-\left(\beta_n^2+\kappa_s^2+\kappa_{d_1}^2\right)\chi_f\right)}},\\&|\mathcal{H}|^2\geq\sqrt{\frac{\chi_n}{\Upsilon_s\left(\beta_n^2-\left(\xi\,\beta_f^2+\kappa_s^2+\kappa_{d_1}^2\right)\chi_n\right)}}\Bigg\},\end{aligned} \tag{45}$$

equivalently,

$$\begin{aligned}P_n&=1-\mathbb{P}\left\{|\mathcal{H}|^2\geq\mathcal{Y}_1,|\mathcal{H}|^2\geq\mathcal{Y}_2\right\},\\&=\mathbb{P}\left\{|\mathcal{H}|^2\leq\mathcal{Y}\right\},\end{aligned} \tag{46}$$

where

$$\mathcal{Y}_1=\frac{\chi_f}{\Upsilon_s\left(\beta_f^2-\left(\beta_n^2+\kappa_s^2+\kappa_{d_1}^2\right)\chi_f\right)}, \tag{47}$$

$$\begin{aligned}\hat{R}_n=\log_2\Bigg[&1+\Xi_1\mathcal{B}_h+2M\,\Xi_1\frac{\Gamma\left(m+\frac{1}{2}\right)}{\Gamma(m)}\sqrt{\frac{\varphi_1^2\,\pi^3\mathcal{B}_h\mathcal{B}_{h_1}\mathcal{B}_{h_2}}{8m\,(K_1+1)(K_2+1)}}L_{\frac{1}{2}}(-K_1)L_{\frac{1}{2}}(-K_2)\\&+M^2\,\Xi_1\,\mathcal{B}_{h_1}\mathcal{B}_{h_2}\frac{\varphi_1^2\,\pi^2}{4\,(K_1+1)(K_2+1)}\left\{L_{\frac{1}{2}}(-K_1)\right\}^2\left\{L_{\frac{1}{2}}(-K_2)\right\}^2\Bigg]\\-\log_2\Bigg[&1+\Xi_2\mathcal{B}_h+2M\,\Xi_2\frac{\Gamma\left(m+\frac{1}{2}\right)}{\Gamma(m)}\sqrt{\frac{\varphi_1^2\,\pi^3\mathcal{B}_h\mathcal{B}_{h_1}\mathcal{B}_{h_2}}{8m\,(K_1+1)(K_2+1)}}L_{\frac{1}{2}}(-K_1)L_{\frac{1}{2}}(-K_2)\\&+M^2\,\Xi_2\,\mathcal{B}_{h_1}\mathcal{B}_{h_2}\frac{\varphi_1^2\,\pi^2}{4\,(K_1+1)(K_2+1)}\left\{L_{\frac{1}{2}}(-K_1)\right\}^2\left\{L_{\frac{1}{2}}(-K_2)\right\}^2\Bigg]\end{aligned} \tag{36}$$

$$\mathcal{Y}_2 = \frac{\chi_n}{\Upsilon_s \left(\beta_n^2 - \left(\xi\, \beta_f^2 + \kappa_s^2 + \kappa_{d_1}^2\right) \chi_n\right)}, \tag{48}$$

and

$$\mathcal{Y} = \max\left\{\mathcal{Y}_1, \mathcal{Y}_2\right\}. \tag{49}$$

Now since the PDF of $|\mathcal{H}|^2$ is not known, hence, P_n does not admit a closed-form solution. However, it can be evaluated through simulations.

Similarly, the outage probability for the FU can be defined as

$$\begin{aligned} P_f &= \mathbb{P}\left\{R_f < R_{th,f}\right\}, \\ &= \mathbb{P}\left\{\log_2(1 + SDINR_f) < R_{th,f}\right\}, \end{aligned} \tag{50}$$

Lemma 3: For the considered RIS-aided NOMA network, the OP for the FU can be expressed as

$$P_f = \frac{\gamma\left(m, \frac{m}{\mu^2}\mathcal{Y}_f\right)}{\Gamma(m)}, \tag{51}$$

where $\mathcal{Y}_f = \sqrt{\frac{\chi_f}{\mathcal{B}_{g_1}\mathcal{B}_{g_2} M^2 \Upsilon_s(\beta_f^2 - (\beta_n^2 + \kappa_s^2 + \kappa_{d_2}^2)\chi_f)}}$, $\chi_f = 2^{R_{th,f}} - 1$.

Proof: Please refer to Appendix C. ■

Remark 12: Likewise, for the RIS-aided OMA scenario, the OP for the FU can be expressed as

$$P_f^O = \frac{\gamma\left(m, \frac{m}{\mu^2}\mathcal{Y}_f^O\right)}{\Gamma(m)}, \tag{52}$$

where $\mathcal{Y}_f^O = \sqrt{\frac{\chi_f}{\mathcal{B}_{g_1}\mathcal{B}_{g_2} M^2 \Upsilon_s(1 - (\kappa_s^2 + \kappa_{d_2}^2)\chi_f)}}$.

C. SPECTRAL EFFICIENCY AND ENERGY EFFICIENCY

The SE of the RIS-aided NOMA system can be defined based on the ergodic rate found in the previous subsection as

$$SE = \bar{R}_n + \bar{R}_f. \tag{53}$$

Remark 13: Since, in the RIS-aided OMA scenario, the two users are orthogonally transmitted in two equal time slots, the SE of the RIS-aided OMA system can be given as

$$SE^O = \frac{1}{2}\left[\bar{R}_n^O + \bar{R}_f^O\right]. \tag{54}$$

Now, the EE can be defined in terms of bits/Joule/Hz as the ratio of the SE and the total power consumed, P_{tot}, which includes power consumed at BS, RIS and the NOMA user pair. Representing the static and dynamic power consumption at the BS as P_{BS} and αP_s, respectively, further, representing the power consumed at the REs as P_{RE} and the power consumed at the users as P_U, the EE can be expressed as

$$EE = \frac{SE}{P_{tot}} = \frac{SE}{(1+\alpha)P_s + P_{BS} + 2MP_{RE} + 2P_U}. \tag{55}$$

Likewise, the EE for the RIS-aided OMA network can also be evaluated.

TABLE III Simulation Parameters

Parameter	Simulation Values
Shape Parameter	K_1, K_3 = 5, K_2, K_4 = 5
Scale Parameter	$\Omega_1 = \Omega_2 = \Omega_3 = \Omega_4 = 1$
Circuit Power	P_{BS}=10 dBm, P_U=10 dBm [19]
RIS Power Consumption	P_{RE} = 10 dBm [19]
Variance of AWGN Noise	σ^2 = -120 dBm
Antenna Gain	G_t = 1, G_r = 1
HPA Power Consumption Factor	α = 1.2 [57]

This completes the analytical evaluation of the proposed RIS-aided NOMA and OMA network. The following remarks are noteworthy here that provide system-design insights and can be summarized as 1) The performance analysis of the designed system provides insights regarding the suitable number of REs, which can be determined to strike a balance between hardware cost and system performance for different scenarios, i.e., downlink (or uplink) NOMA (or OMA). 2) The analytical results contribute to the deployment of RISs under realistic scenarios, i.e., the BS-RIS and RIS-user links can be either LoS or NLoS. 3) Based on the impact of transceiver impairments on the system performance, we know how the non-ideal transceiver limits the performance gain provided by RIS. 4) Further, the impact of the fixed power-allocation coefficients for the different use case scenarios of downlink NOMA.

V. SIMULATION RESULT

This section discusses and presents the simulation results for the performance of both ideal and non-ideal transceiver-based RIS-aided NOMA systems. The general rate threshold used for simulation of near and far user are $R_{th,n} = 5$ and $R_{th,f} = 1.5$ bits per channel use (BPCU), respectively, if not specified. Also, for simulation purposes, the number of users is set to be 2, with the power allocation coefficients of $\beta_n^2 = 0.3$ and $\beta_f^2 = 0.7$, if not specified otherwise. Likewise, the proportionality constant for hardware impairment level is assumed to be $\kappa = 0.1$, where ($\kappa = \kappa_s = \kappa_d$), if not specified otherwise. Further, the distance between the BS-to-RIS and RIS-to-NU is assumed to be 10 m, while the distance between BS-to-NU is 17.32 m. Likewise, for the FU, the distances between BS-to-RIS and RIS-to-FU are supposed to be 40 and 10 m, respectively. The rest of the simulation parameters are summarized in Table III. Further, the proposed RIS-aided NOMA is compared with full-duplex relaying (FDR), where a full-duplex relay is substituted for the RIS. For the sake of fair comparison, the total transmitted power is kept equal in both RIS-aided and FDR-aided NOMA systems. Moreover, in the FDR-aided NOMA system, the transmit power is assumed to be equally distributed at the BS and the full-duplex relay. In addition to the above, solid lines show the analytical results, while the marker points denote the simulation results; a similar convention is followed throughout this section.

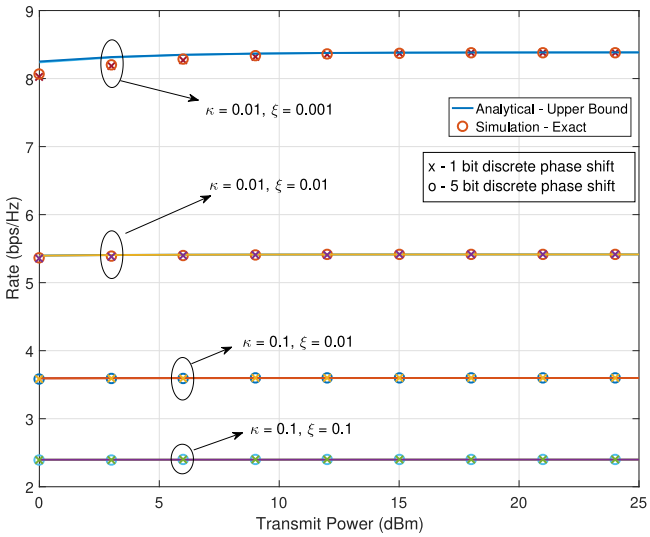

FIGURE 3. Ergodic rate for the NU with respect to transmit power under varying level of hardware impairments, here $M = 10$.

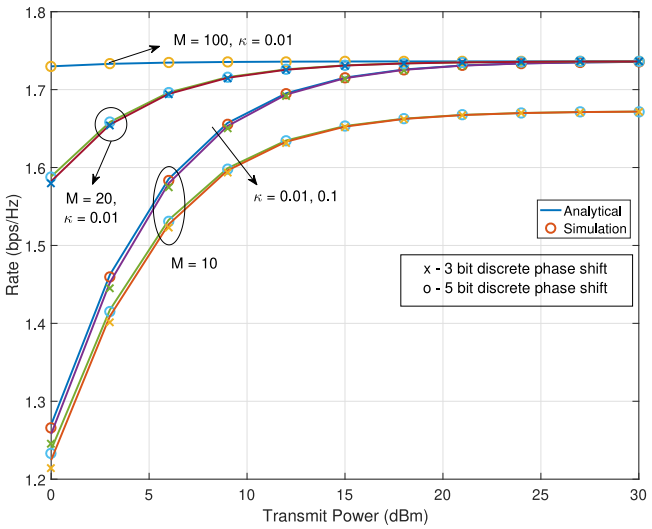

FIGURE 4. Ergodic rate for the FU with respect to transmit power under varying level of hardware impairment.

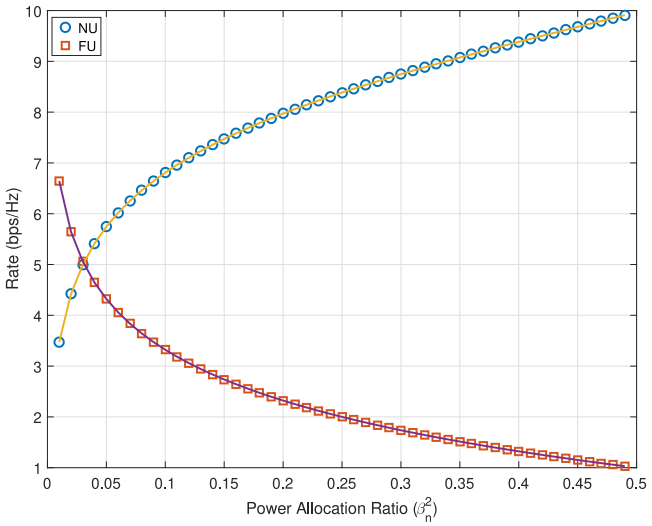

FIGURE 5. Impact of power allocation coefficient on the rate of both the users viz. NU and FU, here $M = 10$, $q = 3$, $P_s = 10$ dBm.

A. SE

Fig. 3 shows the non-ideal hardware's impact on the NU rate in the RIS-aided NOMA wireless system. Specifically, the figure shows the ergodic rate for the NU with respect to the transmit power under the varying level of hardware impairments. The following observations can easily be made from Fig. 3: a) The result shows that the rate of NU saturates with increasing transmit power for the non-ideal hardware-based RIS-aided NOMA system. b) The impact of distortion noise is far more significant than the impact of the phase noise. c) Likewise, the imperfect SIC has a detrimental impact on the ergodic rate of the NU, which is also far more significant than the RIS phase error. d) It can also be observed here that analytical and simulation results are pretty close. This shows that the derived upper bound on the ergodic rate of FU is very tight, specifically in the higher transmit power regime.

Likewise, Fig. 4 shows the ergodic rate of the FU for the RIS-aided NOMA wireless system. The result shows that the rate of FU saturates with increasing transmit power. Further, it can also be observed that for large M, the SE saturates for the lower transmit power values. For instance, FU's rate is 1.55 bps/Hz for $q = 3$, $\kappa = 0.01$ and $M = 10$ at 5 dBm of transmit power, while it saturates at 1.73 bps/Hz at 20 dBm of transmit power. A similar rate can also be achieved at 5 dBm of transmit power by increasing M to 100. Though the rate of FU saturates with respect to transmit power, RIS provides the leverage to tradeoff the transmit power in terms of M. Thus, RIS provides better EE even for the hardware-impaired wireless system. Furthermore, it can also be observed here that the impact of phase error is insignificant as compared to the impact of the non-ideal transceiver and imperfect SIC.

Fig. 5 shows the impact of power allocation co-efficient on the NOMA users' SE. It can be observed that power allocation plays a significant role in the overall SE of the NOMA system. Specifically, it can be observed that to enhance the sum rate, the power allocation for the near user should be more as compared to the far user. This is because the near user has better channel conditions; thus, to maximize the sum rate, the user with better channel conditions should be allocated more power. For instance, at higher values of β_n^2, the rate experienced by the near user is much better than the far user, as evident from this result. In contrast, if fairness between the users is to be ensured, then as can be seen here, the near user should be allocated lesser power, while the far user should be allocated more power. For instance, when $\beta_n^2 = 0.03$, the users' rate is equal to 5 bps/Hz.

Fig. 6 shows the impact of the hardware impairments on the SE of both the RIS-aided NOMA and OMA systems. It can be seen that, for the ideal transceiver ($\kappa = 0$) based on RIS-aided NOMA and OMA, the SE increases with the transmit power linearly. However, as the level of hardware impairment rises,

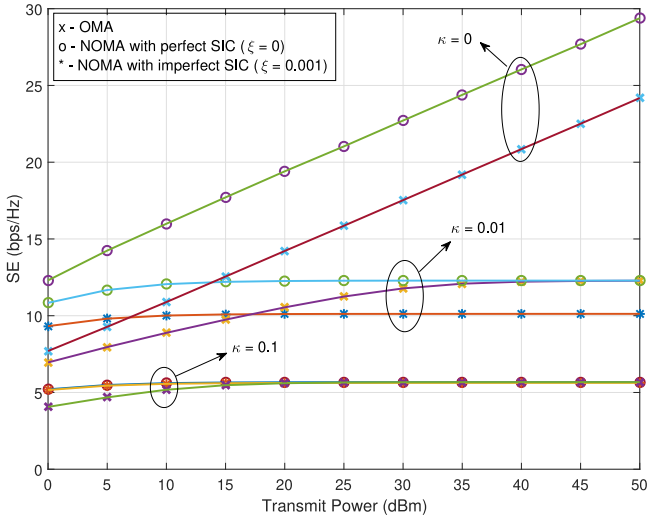

FIGURE 6. SE with respect to transmit power for both RIS-aided NOMA and OMA, here $q = 3$ and $M = 10$.

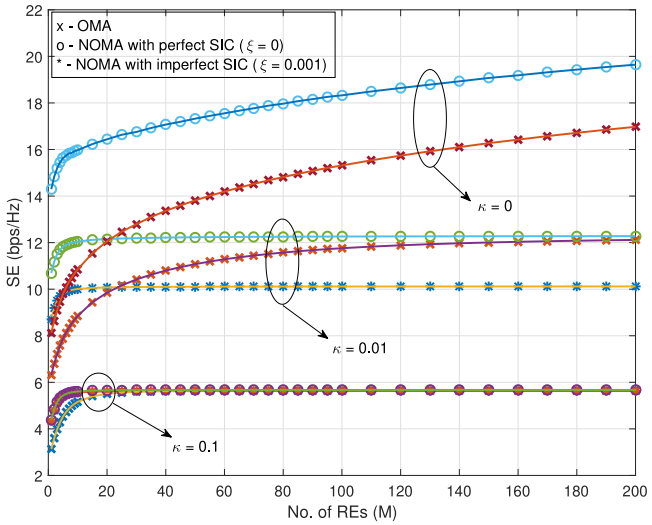

FIGURE 7. SE with respect to M for different level of hardware impairment, here $q = 3$ and $P_s = 10$ dBm.

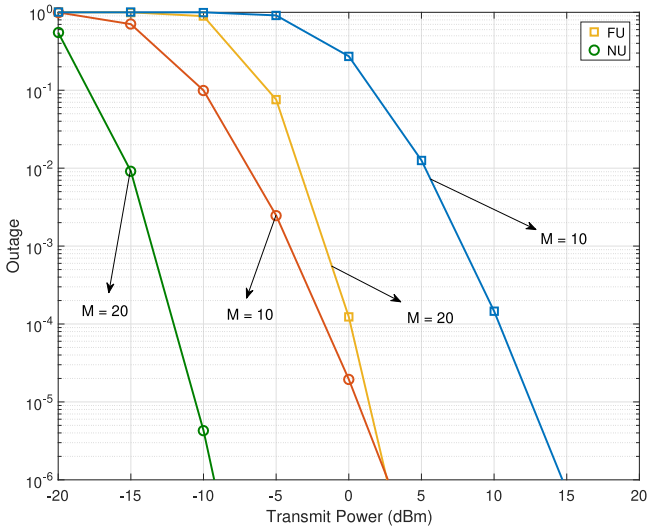

FIGURE 8. Outage with respect to transmit power for both NU and FU of the RIS-aided NOMA System, here $q = 3$, $\xi = 0.001$ and $\kappa = 0.01$.

the SE saturates. For instance, the SE saturates at 12.6 bps/Hz and 5.6 bps/Hz for κ =0.01 and 0.1, respectively. NOMA provides some SE gain over OMA in the moderate transmit power regime. However, at higher power, the SE of both RIS-aided NOMA and OMA saturates. After saturation, no further gain in the SE can be achieved by increasing the transmit power. Specifically, in the high transmit power saturation regime, NOMA provides a gain of around 2.2 bps/Hz in the SE as compared to OMA for the ideal hardware-based system. In comparison, for the hardware-impaired non-ideal system, the SE gain diminishes with increasing transmit power.

Likewise, Fig. 7 shows the SE for the RIS-aided NOMA and OMA system for an increasing number of REs. It can be observed here that SE also saturates with an increasing number of REs for both NOMA and OMA-based system when there is a non-ideal hardware-based system. However, for an ideal hardware scenario, the SE increases linearly. After saturation, no further gain in the SE can be achieved irrespective of the number of REs in the RIS. For instance, the SE saturates at 5.6 bps/Hz for both NOMA and OMA systems at $\kappa = 0.1$, increasing linearly with the number of REs for ideal transceiver-based RIS-aided NOMA and OMA. This shows the detrimental impact of the non-ideal transceiver as the SE is independent of the number of REs in the non-ideal transceiver-based NOMA system. Also, the impact of hardware distortion at the transceivers is far more significant than RIS phase error. Further, it can also be observed that despite a non-ideal transceiver, the NOMA system outperforms the OMA scenario, as evident from the results. Thus, the impact of non-idealities in the transceiver is significant and cannot be ignored while analyzing the performance of RIS-aided wireless networks.

B. OUTAGE

Fig. 8 shows the outage performance of both the NOMA users in the presence of hardware impairments. As evident from the result, the outage performance of the NU is better in the low transmit power regime. While increasing the transmit power, the outage for the FU also improves. For instance, the outage at 5 dBm transmit power for the FU is 0.01, whereas the outage improves to $10^{-}6$ at 15 dBm of transmit power. However, increasing M to 20, a similar outage performance can be observed for the FU at 5 dBm transmit power. Thus, the transmit power can be reduced by increasing M without compromising the quality of service (QoS). Likewise, the outage probability can be enhanced by increasing M for the NU since the FU experiences more attenuation as the distance is considerable for FU compared to NU.

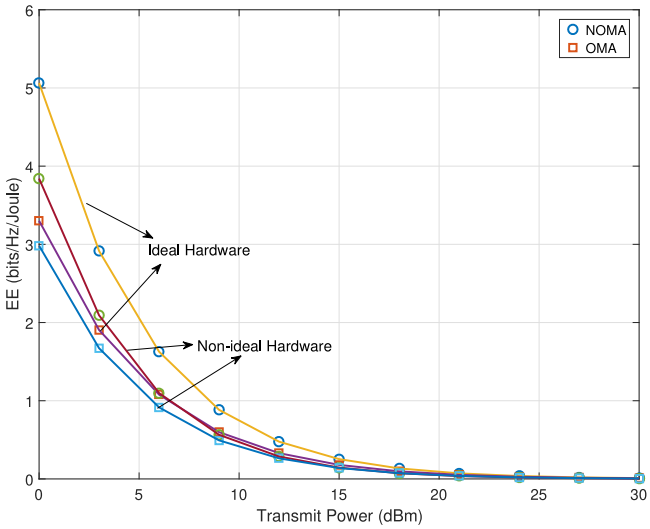

FIGURE 9. EE with respect to transmit power for both RIS-aided NOMA and OMA considering ideal and non-ideal system.

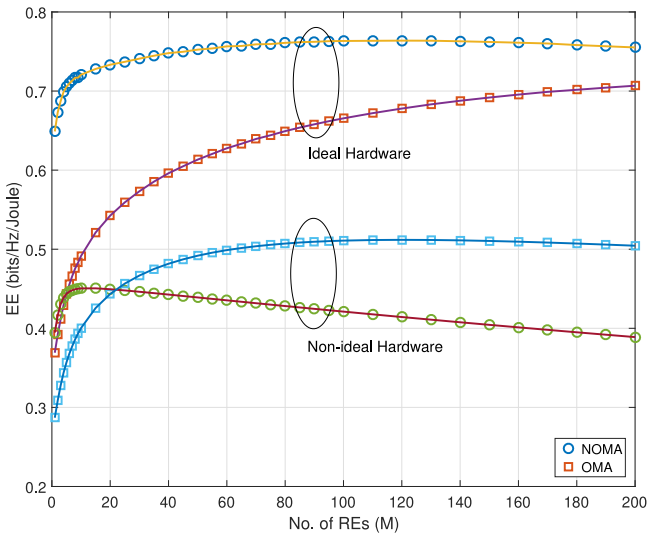

FIGURE 10. EE with respect to varying number of reflecting elements for both RIS-aided NOMA and OMA with ideal and non-ideal system.

C. EE

Fig. 9 and 10 show the EE for both NOMA and OMA scenarios with ideal and non-ideal transceivers. It can be observed that NOMA is more energy-efficient than OMA for both the ideal and non-ideal hardware-based scenarios when the number of REs is small. However, for large REs, RIS-aided OMA may outperform RIS NOMA in EE. Further, it is also evident from the result that the EE of ideal hardware-based RIS-aided NOMA saturates with the number of REs in the RIS. In contrast, for the non-ideal hardware-based RIS-aided NOMA system, the EE decreases with increasing M. This is because of the fact that SE saturates for the non-ideal hardware-based RIS-aided NOMA system while the power consumption increases with M. Thus, the compound effect results in a decrease in the EE of the RIS-aided NOMA system. In contrast, for the ideal transceiver-based RIS-aided NOMA system, the EE improves with the number of REs. However, for a large number of REs, the EE is also saturated, and no significant gain is observed afterward. For instance, the EE at $M = 20$ is 0.73 bits/Hz/Joule for RIS-aided NOMA and 0.55 bits/Hz/Joule for the RIS-aided OMA system. After that, the EE saturates along with the number of REs for NOMA and increases linearly for the OMA system. For instance, when M is increased to 50, the EE remains 0.76 bits/Hz/Joule for NOMA and increases to 0.62 bits/Hz/Joule for OMA from the earlier values (when $M = 20$). This is because the SE is saturated, and the power consumption increases linearly, as evident from (55). Hence, it results in a decrease in the EE of the RIS-aided NOMA system. Further, it also proves that increasing the number of REs does not yield the best performance as the SE saturates and EE decreases, unlike the ideal hardware case, where the SE increases and the EE is saturated. Thus, it can be concluded that the RIS-aided NOMA system outperforms the OMA system in both SE and EE. Further, it is evident that a non-ideal transceiver's impact is much more significant on both the SE and EE, both of which are limited by the distortion noise and imperfect SIC due to non-ideal hardware.

TABLE IV Evaluation Matrix

Simulation Parameter	Ideal Hardware		Non-Ideal Hardware	
	SE	EE	SE	EE
$M = 10$, NOMA	15.98	0.72	10.01	0.45
$M = 10$, OMA	10.86	0.49	8.85	0.40
$M = 100$, NOMA	18.34	0.76	10.12	0.42
$M = 100$, OMA	15.32	0.67	11.76	0.51

Table IV compares ideal and non-ideal hardware-based RIS-aided NOMA wireless transmission systems. It can be inferred here that the ideal transceiver-based RIS-aided NOMA and OMA system have the best EE, whereas the non-ideal transceiver-based RIS-aided NOMA and OMA system have the worse EE. Further, it can also be concluded from the above result that the gain provided by RIS is saturated due to distortion. Thus the non-ideal transceiver significantly impacts the performance of the RIS-aided NOMA and OMA wireless system. So, non-ideal hardware impairments can not be neglected in a practical deployment of RIS-based wireless systems. Finally, it can also be verified from the results that NOMA based system outperforms the OMA-based RIS-aided wireless system.

D. COMPARISON WITH FD RELAYING

Fig. 11 shows the performance comparison of the RIS-aided NOMA network with FDR aided NOMA network. Specifically, as a performance benchmark, the RIS is replaced with a full-duplex (FD) relay, and the FD relay aids the transmission instead of the RIS. It shows that the RIS outperforms the FDR,

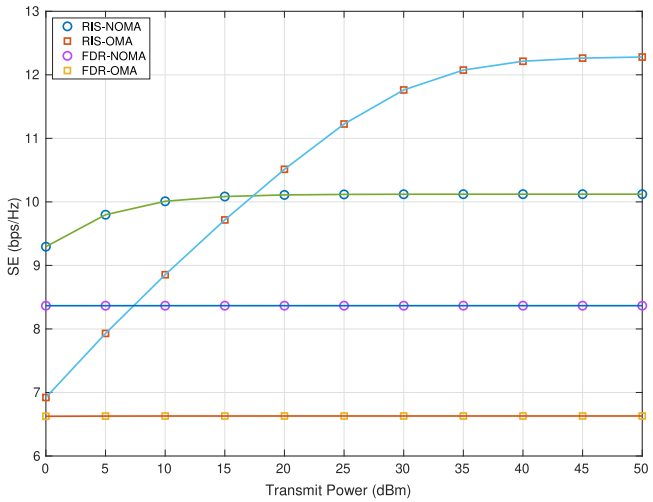

FIGURE 11. SE with respect to transmit power for both OMA and NOMA considering RIS-aided and FDR-aided network.

as evident from the SE result. However, as discussed earlier, the hardware impairment due to the non-ideal transceiver saturates the performance of FDR-aided NOMA and OMA. Further, it can also be observed that the FD-aided NOMA scenario provides more SE than the FD-aided OMA counterpart for the FDR-aided network. Similarly, it can be observed here that a RIS-aided OMA network also performs better than the FDR-aided OMA network. This shows the RIS-aided NOMA system's potential within the existing wireless systems.

VI. CONCLUSION

In this paper, we investigated the impact of the non-ideal transceiver on the performance of a RIS-aided NOMA system. Specifically, we derived the closed-form expressions for OP, SE and EE in the presence of a non-ideal transceiver. Further, the performance of the NOMA system is compared with its OMA counterpart, where the results show that the RIS-aided NOMA system outperforms the OMA scenario in both SE and EE. Also, the result shows that the SE saturates in the non-ideal transceiver-based NOMA system, and this saturation level is independent of the number of REs in the RIS. Further, the EE decreases with the number of REs. In contrast, the SE of an ideal system increases with the number of REs, whereas the EE also increases but saturates for a very large number of REs. Thus, the impact of the non-ideal transceiver can not be overlooked while designing the practical RIS-aided NOMA system. In addition to the above, we also compared the performance of the RIS-aided system with the FDR-aided network, where it has been shown that the RIS-aided network significantly outperforms the FDR-aided network.

ACKNOWLEDGMENT

This publication is an outcome of the research and development work undertaken project under the Visvesvaraya PhD Scheme of Ministry of Electronics Information Technology, Government of India, being implemented by Digital India Corporation.

APPENDIX A
PROOF OF LEMMA 1

The ergodic rate for FU can be evaluated from (30) as,

$$\bar{R}_f = \mathbb{E}\left[\log_2\left(1 + SDINR_f\right)\right], \tag{56}$$

where $SDINR_f$ can be further expanded as

$$SDINR_f = \frac{\mathcal{B}_{g_1}\mathcal{B}_{g_2}\ |\mathcal{G}|^2\ \beta_f^2\,\Upsilon_s}{\mathcal{B}_{g_1}\mathcal{B}_{g_2}\ |\mathcal{G}|^2\ \left(\beta_n^2 + \kappa_s^2 + \kappa_{d_2}^2\right)\Upsilon_s + 1}, \tag{57}$$

which can be re-written as

$$SDINR_f = \frac{M^2\,\mathcal{B}\ |G|^2\ \beta_f^2\,\Upsilon_s}{M^2\,\mathcal{B}\ |G|^2\ \left(\beta_n^2 + \kappa_s^2 + \kappa_{d_2}^2\right)\Upsilon_s + 1}. \tag{58}$$

where $\mathcal{B}$ is substituted for $\mathcal{B}_{g_1}\mathcal{B}_{g_2}$.

Now the cumulative distribution function (CDF) and the PDF for the channel gain $|G|^2$ can be derived as [29]

$$f_{|\mathcal{G}|^2}(g) = \frac{m^m}{\Gamma(m)\,\mu^{2\,m}} g^{m-1} \exp\left(-\frac{m}{\mu^2} g\right), \tag{59}$$

and

$$F_{|G|^2}(g) = \frac{\gamma\left(m, \frac{m}{\mu^2} g\right)}{\Gamma(m)}, \tag{60}$$

respectively. Here, m and μ are constants, which are defined as

$$m = \frac{M}{2}\frac{\varphi_1^2\,a^4}{1 + \varphi_2 - 2\,\varphi_1^2\,a^4}, \quad \mu = \varphi_1\,a^2, \tag{61}$$

where $a = \sqrt{a_1\,a_2}$ with a_1 and a_2 being the expected values of Rician RV g_1 and g_2, respectively. It can further be noticed that, for a Rician variable $g_1 \in \{0, 1\}$, the expected value can be given as

$$\mathbb{E}\{|g_1|\} = \sqrt{\frac{\pi}{2\,(K_3 + 1)}} L_{\frac{1}{2}}\left(-K_3\right). \tag{62}$$

Utilizing (58) and (59) to solve the expectation in (56), we can have

$$\bar{R}_f = \int_0^\infty \log_2\left(1 + \frac{g\,\mathcal{B}\,M^2\,\beta_f^2\,\Upsilon_s}{g\,\mathcal{B}\,M^2\left(\beta_n^2 + \kappa_s^2 + \kappa_{d_2}^2\right)\Upsilon_s + 1}\right) f_G(g)\mathrm{dg}. \tag{63}$$

Now the ergodic rate for the FU case can be derived by substituting (59) in (63) as

$$\bar{R}_f = \frac{m^m}{\Gamma(m)\,\mu^{2\,m}\,\ln(2)} \int_0^\infty \ln$$

$$\left(1+\frac{g\,\mathcal{B}\,M^2\,\beta_f^2\,\Upsilon_s}{g\,\mathcal{B}\,M^2\left(\beta_n^2+\kappa_s^2+\kappa_{d_2}^2\right)\Upsilon_s+1}\right)g^{m-1}\exp \times\left(-\frac{m}{\mu^2}g\right)\mathrm{dg}, \tag{64}$$

which after simplification and re-arrangement can be expressed as

$$\bar{R}_f=\frac{m^m}{\Gamma(m)\,\mu^{2\,m}\,\ln(2)}\left\{\mathcal{I}_1-\mathcal{I}_2\right\}, \tag{65}$$

where

$$\mathcal{I}_1=\int_0^\infty \ln\left(1+g\mathcal{C}_1\Upsilon_s\right)g^{m-1}\exp\left(-\frac{m}{\mu^2}g\right)\mathrm{dg}, \tag{66}$$

and

$$\mathcal{I}_2=\int_0^\infty \ln\left(1+g\mathcal{C}_2\Upsilon_s\right)g^{m-1}\exp\left(-\frac{m}{\mu^2}g\right)\mathrm{dg}, \tag{67}$$

with $\mathcal{C}_1=\mathcal{B}M^2\left(1+\kappa_s^2+\kappa_{d_2}^2\right)$ and $\mathcal{C}_2=\mathcal{B}M^2\left(\beta_n^2+\kappa_s^2+\kappa_{d_2}^2\right)$.

Now $\mathcal{I}_1$ and $\mathcal{I}_2$ can be solved by utilizing [28, 17] and can be expressed as shown in (68) and (69) shown at the bottom of this page. Further, $\mathcal{I}_1$ and $\mathcal{I}_2$ can be substituted in (65) to get the expression for $\bar{R}_f$, as shown in (31).

APPENDIX B
PROOF OF LEMMA 2

Since the closed form PDF is not available for the channel gain of NU, i.e., $\mathcal{H}$. We can evaluate an upper bound on the ergodic rate of NU, $\bar{R}_n$. From (29), the rate can be re-written as

$$\bar{R}_n=\mathbb{E}\left[\log_2\left(1+\frac{|\mathcal{H}|^2\,\beta_n^2\,\Upsilon_s}{|\mathcal{H}|^2\left(\xi\,\beta_f^2+\kappa_s^2+\kappa_{d_1}^2\right)\Upsilon_s+1}\right)\right], \tag{70}$$

which can be modified as

$$\bar{R}_n=\mathbb{E}\left[\log_2\left(\frac{1+|\mathcal{H}|^2\left(\xi\,\beta_f^2+\kappa_s^2+\kappa_{d_1}^2+\beta_n^2\right)\Upsilon_s}{1+|\mathcal{H}|^2\left(\xi\,\beta_f^2+\kappa_s^2+\kappa_{d_1}^2\right)\Upsilon_s}\right)\right],$$

$$=\mathbb{E}\left[\log_2\left(1+\Xi_1|\mathcal{H}|^2\right)-\log_2\left(1+\Xi_2|\mathcal{H}|^2\right)\right],$$

$$=\mathbb{E}\left[\log_2\left(1+\Xi_1|\mathcal{H}|^2\right)\right]-\mathbb{E}\left[\log_2\left(1+\Xi_2|\mathcal{H}|^2\right)\right], \tag{71}$$

where Ξ_1 and Ξ_2 are constant defined as $\Xi_1=(\xi\,\beta_f^2+\kappa_s^2+\kappa_{d_1}^2+\beta_n^2)\Upsilon_s$ and $\Xi_2=(\xi\,\beta_f^2+\kappa_s^2+\kappa_{d_1}^2)\Upsilon_s$.

Applying Jensen's inequality, the upper bound for ergodic rate can be evaluated as

$$\bar{R}_n\le\hat{R}_n, \tag{72}$$

where $\hat{R}_n$ can be defined as

$$\hat{R}_n=\log_2\left(1+\Xi_1\mathbb{E}\left[|\mathcal{H}|^2\right]\right)-\log_2\left(1+\Xi_2\mathbb{E}\left[|\mathcal{H}|^2\right]\right). \tag{73}$$

Now in order to evaluate $\mathbb{E}[|\mathcal{H}|^2]$, we apply the binomial expansion theorem here, we have

$$\mathbb{E}\left[|\mathcal{H}|^2\right]=\mathbb{E}\left[\left|\sqrt{\mathcal{B}_h}\,h+\sqrt{\mathcal{B}_{h_1}\mathcal{B}_{h_2}}\;M\;|H|\right|^2\right],$$

$$=\mathcal{B}_h\underbrace{\mathbb{E}\left\{|h|^2\right\}}_{\mathcal{E}_1}+\mathcal{B}_{h_1}\mathcal{B}_{h_2}M^2\underbrace{\mathbb{E}\left\{|H|^2\right\}}_{\mathcal{E}_2}$$

$$+2M\sqrt{\mathcal{B}_h\mathcal{B}_{h_1}\mathcal{B}_{h_2}}\underbrace{\mathbb{E}\left\{|h|\,|H|\right\}}_{\mathcal{E}_3}. \tag{74}$$

We now calculate $\mathcal{E}_1$, $\mathcal{E}_2$ and $\mathcal{E}_3$ one-by-one.

Calculating $\mathcal{E}_1$: Obviously, we have $\mathcal{E}_1=1$, as $h\sim\mathcal{CN}(0,1)$.

Calculating $\mathcal{E}_2$: Now, $\mathbb{E}\{|H|^2\}$ is a Gamma distributed RV (for more details, please refer to Appendix A), so $\mathbb{E}\{|H|^2\}=\mu^2$, which can be given as $\varphi_1^2\,a_1^2\,a_2^2$. Thus, on further expanding,

$$\mathbb{E}\left\{|H|^2\right\}=\frac{\varphi_1^2\,\pi^2}{4\,(K_1+1)\,(K_2+1)}\left\{L_{\frac{1}{2}}(-K_1)\right\}^2\left\{L_{\frac{1}{2}}(-K_2)\right\}^2. \tag{75}$$

Calculating $\mathcal{E}_3$: Now, for the Rayleigh variable $|h|$, we have

$$\mathbb{E}\left\{|h|\right\}=\sqrt{\frac{\pi}{2}}, \tag{76}$$

$$\mathcal{I}_1=\frac{\pi}{(\mathcal{C}_1\,\Upsilon_s)^m}\frac{{}_1F_1\left(m;\,m+1;\,\frac{m}{\mu^2}\frac{1}{\mathcal{C}_1\,\Upsilon_s}\right)}{m\,\sin(m\,\pi)}-\frac{\mu^{2\,m}\,\Gamma(m)}{m^m}\left[\ln\left(\frac{m}{\mu^2}\frac{1}{\mathcal{C}_1\,\Upsilon_s}\right)-\Psi(m)\right.$$

$$\left.+\frac{m}{\mu^2\,(1-m)}\frac{1}{\mathcal{C}_1\,\Upsilon_s}\,{}_2F_2\left(1,1;\,2,2-m;\,\frac{m}{\mu^2}\frac{1}{\mathcal{C}_1\,\Upsilon_s}\right)\right] \tag{68}$$

$$\mathcal{I}_2=\frac{\pi}{(\mathcal{C}_2\,\Upsilon_s)^m}\frac{{}_1F_1\left(m;\,m+1;\,\frac{m}{\mu^2}\frac{1}{\mathcal{C}_2\,\Upsilon_s}\right)}{m\,\sin(m\,\pi)}-\frac{\mu^{2\,m}\,\Gamma(m)}{m^m}\left[\ln\left(\frac{m}{\mu^2}\frac{1}{\mathcal{C}_2\,\Upsilon_s}\right)-\Psi(m)\right.$$

$$\left.+\frac{m}{\mu^2\,(1-m)}\frac{1}{\mathcal{C}_2\,\Upsilon_s}\,{}_2F_2\left(1,1;\,2,2-m;\,\frac{m}{\mu^2}\frac{1}{\mathcal{C}_2\,\Upsilon_s}\right)\right] \tag{69}$$

while $|H|$ is a Nakagami-m RV with

$$\mathbb{E}\{|H|\} = \frac{\Gamma\left(m+\frac{1}{2}\right)}{\Gamma(m)}\sqrt{\frac{\mu^2}{m}}, = \frac{\Gamma\left(m+\frac{1}{2}\right)}{\Gamma(m)}\frac{\varphi_1\,\pi\,L_{\frac{1}{2}}(-K_1)\,L_{\frac{1}{2}}(-K_2)}{\sqrt{4\,m\,(K_1+1)\,(K_2+1)}}. \quad (77)$$

So, $\mathcal{E}_3$ can be expressed as

$$\sqrt{\frac{\varphi_1^2\,\pi^3}{8\,m\,(K_1+1)\,(K_2+1)}}\frac{\Gamma\left(m+\frac{1}{2}\right)}{\Gamma(m)}L_{\frac{1}{2}}(-K_1)\,L_{\frac{1}{2}}(-K_2). \quad (78)$$

Finally, putting $\mathcal{E}_1$, $\mathcal{E}_2$ and $\mathcal{E}_3$ all together yields $\mathbb{E}[|\mathcal{H}|^2]$ which can be expressed as

$$\mathbb{E}\left[|\mathcal{H}|^2\right] = \mathcal{B}_h + M^2\mathcal{B}_{h_1}\mathcal{B}_{h_2}\frac{\varphi_1^2\,\pi^2}{4\,(K_1+1)\,(K_2+1)} \times \left\{L_{\frac{1}{2}}(-K_1)\right\}^2\left\{L_{\frac{1}{2}}(-K_2)\right\}^2 + 2\,M\,\frac{\Gamma\left(m+\frac{1}{2}\right)}{\Gamma(m)} \times \sqrt{\frac{\varphi_1^2\,\pi^3\mathcal{B}_h\mathcal{B}_{h_1}\mathcal{B}_{h_2}}{8\,m\,(K_1+1)\,(K_2+1)}}L_{\frac{1}{2}}(-K_1)\,L_{\frac{1}{2}}(-K_2). \quad (79)$$

which can be put in (73) to give the desired upper bound as shown in (36).

APPENDIX C
PROOF OF LEMMA 3

The OP for the FU can be evaluated from (50), as

$$P_f = \mathbb{P}\left\{SDINR_f < 2^{R_{th,f}} - 1\right\}, = \mathbb{P}\left\{SDINR_f < \chi_f\right\}, \quad (80)$$

which on substituting $SDINR_f$ from (58) gives

$$= \mathbb{P}\left\{\frac{g\,\mathcal{B}\,M^2\,\beta_f^2\,\Upsilon_s}{g\,\mathcal{B}\,M^2\left(\beta_n^2+\kappa_s^2+\kappa_{d_2}^2\right)\Upsilon_s + 1} < \chi_f\right\}. \quad (81)$$

After simplification, (81) can be re-written as

$$P_f = \mathbb{P}\left\{g < \sqrt{\frac{\chi_f}{\mathcal{B}\,M^2\,\Upsilon_s\left(\beta_f^2 - (\beta_n^2+\kappa_s^2+\kappa_{d_2}^2)\chi_f\right)}}\right\}, \quad (82)$$

$$= \mathbb{P}\left\{g < \mathcal{Y}_f\right\}, \quad (83)$$

where

$$\mathcal{Y}_f = \sqrt{\frac{\chi_f}{\mathcal{B}\,M^2\,\Upsilon_s\left(\beta_f^2 - (\beta_n^2+\kappa_s^2+\kappa_{d_2}^2)\chi_f\right)}}. \quad (84)$$

Next, from (59), the outage probability,P_f, can be evaluated as

$$P_{out} = \int_0^{\mathcal{Y}_f} f_G(g)\mathrm{dg}, \quad (85)$$

or, equivalently

$$P_{out} = F_G(\mathcal{Y}_f), \quad (86)$$

which can be expressed as shown in (52).

REFERENCES

[1] W. Jiang, B. Han, M. A. Habibi, and H. D. Schotten, "The road towards 6G: A comprehensive survey," *IEEE Open J. Commun. Soc.*, vol. 2, pp. 334–366, 2021.

[2] "6G: The next hyper-connected experience for all," Samsung Research, Tech. Rep., 2020.

[3] G. Gui, M. Liu, F. Tang, N. Kato, and F. Adachi, "6G: Opening new horizons for integration of comfort, security, and intelligence," *IEEE Wireless Commun.*, vol. 27, no. 5, pp. 126–132, Oct. 2020.

[4] L. Bariah et al., "A prospective look: Key enabling technologies, applications and open research topics in 6G networks," *IEEE Access*, vol. 8, pp. 174792–174820, 2020.

[5] M. Z. Chowdhury, M. Shahjalal, S. Ahmed, and Y. M. Jang, "6G wireless communication systems: Applications, requirements, technologies, challenges, and research directions," *IEEE Open J. Commun. Soc.*, vol. 1, pp. 957–975, 2020.

[6] H. He, X. Yu, J. Zhang, S. Song, and K. B. Letaief, "Cell-free massive MIMO for 6G wireless communication networks," *J. Commun. Info. Netw.*, vol. 6, no. 4, pp. 321–335, Dec. 2021.

[7] B. Clerckx, J. Kim, K. W. Choi, and D. I. Kim, "Foundations of wireless information and power transfer: Theory, prototypes, and experiments," *Proc. IEEE*, vol. 110, no. 1, pp. 8–30, Jan. 2022.

[8] Y. Zeng, Q. Wu, and R. Zhang, "Accessing from the sky: A tutorial on UAV communications for 5G and beyond," *Proc. IEEE*, vol. 107, no. 12, pp. 2327–2375, Dec. 2019.

[9] M. H. N. Shaikh, V. A. Bohara, P. Aggarwal, and A. Srivastava, "Energy efficiency evaluation for downlink full-duplex nonlinear MU-MIMO-OFDM system with self-energy recycling," *IEEE Syst. J.*, vol. 14, no. 3, pp. 3313–3324, Sep. 2020.

[10] N. Rajatheva et al., "White paper on broadband connectivity in 6G," *6G Res. Vis.*, vol. 10, 2020.

[11] H. Elayan, O. Amin, B. Shihada, R. M. Shubair, and M.-S. Alouini, "Terahertz band: The last piece of RF spectrum puzzle for communication systems," *IEEE Open J. Commun. Soc.*, vol. 1, pp. 1–32, 2020.

[12] Q. Wu, S. Zhang, B. Zheng, C. You, and R. Zhang, "Intelligent reflecting surface-aided wireless communications: A tutorial," *IEEE Trans. Commun.*, vol. 69, no. 5, pp. 3313–3351, May 2021.

[13] Q. Wu and R. Zhang, "Intelligent reflecting surface enhanced wireless network via joint active and passive beamforming," *IEEE Trans. Wireless Commun.*, vol. 18, no. 11, pp. 5394–5409, Nov. 2019.

[14] M. Jung, W. Saad, Y. Jang, G. Kong, and S. Choi, "Reliability analysis of large intelligent surfaces (LISs): Rate distribution and outage probability," *IEEE Wireless Commun. Lett.*, vol. 8, no. 6, pp. 1662–1666, Dec. 2019.

[15] S. Hu, F. Rusek, and O. Edfors, "Beyond massive MIMO: The potential of data transmission with large intelligent surfaces," *IEEE Trans. Sig. Process.*, vol. 66, no. 10, pp. 2746–2758, May 2018.

[16] I. Yildirim, A. Uyrus, and E. Basar, "Modeling and analysis of reconfigurable intelligent surfaces for indoor and outdoor applications in future wireless networks," *IEEE Trans. Commun.*, vol. 69, no. 2, pp. 1290–1301, Feb. 2021.

[17] I. Budhiraja et al., "A systematic review on NOMA variants for 5 G and beyond," *IEEE Access*, vol. 9, pp. 85573–85644, 2021.

[18] Y. Huang, C. Zhang, J. Wang, Y. Jing, L. Yang, and X. You, "Signal processing for MIMO-NOMA: Present and future challenges," *IEEE Wireless Commun.*, vol. 25, no. 2, pp. 32–38, Apr. 2018.

[19] C. Huang, A. Zappone, G. C. Alexandropoulos, M. Debbah, and C. Yuen, "Reconfigurable intelligent surfaces for energy efficiency in wireless communication," *IEEE Trans. Wireless Commun.*, vol. 18, no. 8, pp. 4157–4170, Aug. 2019.

[20] C. Pan et al., "Intelligent reflecting surface aided MIMO broadcasting for simultaneous wireless information and power transfer," *IEEE J. Sel. Areas Commun.*, vol. 38, no. 8, pp. 1719–1734, Aug. 2020.

[21] B. Lyu, P. Ramezani, D. T. Hoang, S. Gong, Z. Yang, and A. Jamalipour, "Optimized energy and information relaying in self-sustainable IRS-empowered WPCN," *IEEE Trans. Commun.*, vol. 69, no. 1, pp. 619–633, Jan. 2021.
[22] Y. Chen, Y. Wang, J. Zhang, and Z. Li, "Resource allocation for intelligent reflecting surface aided vehicular communications," *IEEE Trans. Veh. Tech.*, vol. 69, no. 10, pp. 12321–12326, Oct. 2020.
[23] J. Chen, Y.-C. Liang, Y. Pei, and H. Guo, "Intelligent reflecting surface: A programmable wireless environment for physical layer security," *IEEE Access*, vol. 7, pp. 82599–82612, 2019.
[24] A. A. Boulogeorgos and A. Alexiou, "How much do hardware imperfections affect the performance of reconfigurable intelligent surface-assisted systems?," *IEEE Open J. Commun. Soc.*, vol. 1, pp. 1185–1195, 2020.
[25] M. H. N. Shaikh, V. A. Bohara, A. Srivastava, and G. Ghatak, "Performance analysis of intelligent reflecting surface-assisted wireless system with non-ideal transceiver," *IEEE Open J. Commun. Soc.*, vol. 2, pp. 671–686, 2021.
[26] M. H. N. Shaikh, V. A. Bohara, A. Srivastava, and G. Ghatak, "On the performance of RIS-aided NOMA system with non-ideal transceiver over Nakagami-*m* fading," in *Proc. IEEE Wireless Commun. Netw. Conf.*, 2022, pp. 1737–1742.
[27] M. Al-Jarrah, A. Al-Dweik, E. Alsusa, Y. Iraqi, and M.-S. Alouini, "On the performance of IRS-assisted multi-layer UAV communications with imperfect phase compensation," *IEEE Trans. Commun.*, vol. 69, no. 12, pp. 8551–8568, Dec. 2021.
[28] M. Al-Jarrah, E. Alsusa, A. Al-Dweik, and D. K. C. So, "Capacity analysis of IRS-based UAV communications with imperfect phase compensation," *IEEE Wireless Commun. Lett.*, vol. 10, no. 7, pp. 1479–1483, Jul. 2021.
[29] M.-A. Badiu and J. P. Coon, "Communication through a large reflecting surface with phase errors," *IEEE Wireless Commun. Lett.*, vol. 9, no. 2, pp. 184–188, Feb. 2020.
[30] S. Abeywickrama, R. Zhang, Q. Wu, and C. Yuen, "Intelligent reflecting surface: Practical phase shift model and beamforming optimization," *IEEE Trans. Commun.*, vol. 68, no. 9, pp. 5849–5863, 2020.
[31] E. Björnson, ö. özdogan, and E. G. Larsson, "Intelligent reflecting surface versus decode-and-forward: How large surfaces are needed to beat relaying?," *IEEE Wireless Commun. Lett.*, vol. 9, no. 2, pp. 244–248, Feb. 2020.
[32] M. Di Renzo et al., "Smart radio environments empowered by reconfigurable intelligent surfaces: How it works, state of research, and the road ahead," *IEEE J. Sel. Areas Commun.*, vol. 38, no. 11, pp. 2450–2525, Nov. 2020.
[33] E. Basar, M. Di Renzo, J. De Rosny, M. Debbah, M.-S. Alouini, and R. Zhang, "Wireless communications through reconfigurable intelligent surfaces," *IEEE Access*, vol. 7, pp. 116753–116773, 2019.
[34] Q. Wu and R. Zhang, "Towards smart and reconfigurable environment: Intelligent reflecting surface aided wireless network," *IEEE Commun. Mag.*, vol. 58, no. 1, pp. 106–112, Jan. 2020.
[35] C. Liaskos, S. Nie, A. Tsioliaridou, A. Pitsillides, S. Ioannidis, and I. Akyildiz, "A new wireless communication paradigm through software-controlled metasurfaces," *IEEE Commun. Mag.*, vol. 56, no. 9, pp. 162–169, Sep. 2018.
[36] A. S. d. Sena, D. Carrillo, F. Fang, P. H. J. Nardelli, D. B. d. Costa, U. S. Dias, Z. Ding, C. B. Papadias, and W. Saad, "What role do intelligent reflecting surfaces play in multi-antenna non-orthogonal multiple access?," *IEEE Wireless Commun.*, vol. 27, no. 5, pp. 24–31, Oct. 2020.
[37] Z. Ding and H. Vincent Poor, "A simple design of IRS-NOMA transmission," *IEEE Commun. Lett.*, vol. 24, no. 5, pp. 1119–1123, May 2020.
[38] F. Fang, Y. Xu, Q. V. Pham, and Z. Ding, "Energy-efficient design of IRS-NOMA networks," *IEEE Tran. Veh. Tech.*, vol. 69, no. 11, pp. 14088–14092, Nov. 2020.
[39] T. Hou, Y. Liu, Z. Song, X. Sun, Y. Chen, and L. Hanzo, "Reconfigurable intelligent surface aided NOMA networks," *IEEE J. Sel. Areas Commun.*, vol. 38, no. 11, pp. 2575–2588, Nov. 2020.
[40] Y. Cheng, K. H. Li, Y. Liu, K. C. Teh, and H. Vincent Poor, "Downlink and uplink intelligent reflecting surface aided networks: NOMA and OMA," *IEEE Trans. Wireless Commun.*, vol. 20, no. 6, pp. 3988–4000, Jun. 2021.
[41] J. Zhu, Y. Huang, J. Wang, K. Navaie, and Z. Ding, "Power efficient IRS-assisted NOMA," *IEEE Trans. Commun.*, vol. 69, no. 2, pp. 900–913, Feb. 2021.
[42] X. Mu, Y. Liu, L. Guo, J. Lin, and N. Al-Dhahir, "Exploiting intelligent reflecting surfaces in NOMA networks: Joint beamforming optimization," *IEEE Trans. Wireless Commun.*, vol. 19, no. 10, pp. 6884–6898, Oct. 2020.
[43] J. Zuo, Y. Liu, Z. Qin, and N. Al-Dhahir, "Resource allocation in intelligent reflecting surface assisted NOMA systems," *IEEE Trans. Commun.*, vol. 68, no. 11, pp. 7170–7183, Nov. 2020.
[44] T. Hou, Y. Liu, Z. Song, X. Sun, and Y. Chen, "MIMO-NOMA networks relying on reconfigurable intelligent surface: A signal cancellation-based design," *IEEE Trans. Commun.*, vol. 68, no. 11, pp. 6932–6944, Nov. 2020.
[45] A. Hemanth, K. Umamaheswari, A. C. Pogaku, D.-T. Do, and B. M. Lee, "Outage performance analysis of reconfigurable intelligent surfaces-aided NOMA under presence of hardware impairment," *IEEE Access*, vol. 8, pp. 212156–212165, 2020.
[46] C. Wu, Y. Liu, X. Mu, X. Gu, and O. A. Dobre, "Coverage characterization of STAR-RIS networks: NOMA and OMA," *IEEE Commun. Lett.*, vol. 25, no. 9, pp. 3036–3040, Sep. 2021.
[47] A.-T. Le, N.-D. X. Ha, D.-T. Do, A. Silva, and S. Yadav, "Enabling user grouping and fixed power allocation scheme for reconfigurable intelligent surfaces-aided wireless systems," *IEEE Access*, vol. 9, pp. 92263–92275, 2021.
[48] Z. Wang, L. Liu, and S. Cui, "Channel estimation for intelligent reflecting surface assisted multiuser communications: Framework, algorithms, and analysis," *IEEE Trans. Wireless Commun.*, vol. 19, no. 10, pp. 6607–6620, Oct. 2020.
[49] Z.-Q. He and X. Yuan, "Cascaded channel estimation for large intelligent metasurface assisted massive MIMO," *IEEE Wireless Commun. Lett.*, vol. 9, no. 2, pp. 210–214, Feb. 2020.
[50] H. Liu, X. Yuan, and Y.-J. A. Zhang, "Matrix-calibration-based cascaded channel estimation for reconfigurable intelligent surface assisted multiuser MIMO," *IEEE J. Sel. Areas Commun.*, vol. 38, no. 11, pp. 2621–2636, Nov. 2020.
[51] A. M. Salhab and M. H. Samuh, "Accurate performance analysis of reconfigurable intelligent surfaces over rician fading channels," *IEEE Wireless Commun. Lett.*, vol. 10, no. 5, pp. 1051–1055, May 2021.
[52] Q. Tao, J. Wang, and C. Zhong, "Performance analysis of intelligent reflecting surface aided communication systems," *IEEE Commun. Lett.*, vol. 24, no. 11, pp. 2464–2468, Nov. 2020.
[53] A. Papazafeiropoulos, S. K. Sharma, T. Ratnarajah, and S. Chatzinotas, "Impact of residual additive transceiver hardware impairments on rayleigh-product MIMO channels with linear receivers: Exact and asymptotic analyses," *IEEE Trans. Commun.*, vol. 66, no. 1, pp. 105–118, Jan. 2018.
[54] X. Yang, M. Matthaiou, J. Yang, C.-K. Wen, F. Gao, and S. Jin, "Hardware-constrained millimeter-wave systems for 5 G: Challenges, opportunities, and solutions," *IEEE Commun. Mag.*, vol. 57, no. 1, pp. 44–50, Jan. 2019.
[55] I. Trigui, W. Ajib, W.-P. Zhu, and M. D. Renzo, "Performance evaluation and diversity analysis of RIS-assisted communications over generalized fading channels in the presence of phase noise," *IEEE Open J. Commun. Soc.*, vol. 3, pp. 593–607, 2022.
[56] A. S. de Sena et al., "Massive MIMO-NOMA networks with imperfect SIC: Design and fairness enhancement," *IEEE Trans. Wireless Commun.*, vol. 19, no. 9, pp. 6100–6115, Sep. 2020.
[57] M. H. N. Shaikh, V. A. Bohara, and A. Srivastava, "Performance analysis of a full-duplex MIMO decode-and-forward relay system with self-energy recycling," *IEEE Access*, vol. 8, pp. 226248–226266, 2020.

MOHD HAMZA NAIM SHAIKH received the B.Tech. and M.Tech. degrees from Aligarh Muslim University, Aligarh, India, in 2014 and 2016, respectively. He is currently working toward the Ph.D. degree with the Indian Institute of Technology Delhi, New Delhi, India. His research interests include next-generation communication technologies, such as full-duplex, intelligent reflecting surfaces, massive MIMO, and energy-efficient wireless system design.

VIVEK ASHOK BOHARA (Senior Member, IEEE) received the Ph.D. degree from Nanyang Technological University, Singapore, in 2011. From 2011 to 2013, he was a Postdoctoral Researcher (Marie Curie fellowship) in ESIEE Paris, University Paris-East, Champs-sur-Marne, France. In 2013, he joined IIIT-Delhi, India, where he is currently an Associate Professor and Head, Department of Electronics and Communication. He has authored or coauthored more than 50 publications in major IEEE/IET journals and refereed international conferences, two book chapters, and two patents. His research interests include next-generation communication technologies, such as device-to-device communication, carrier aggregation, and Visible Light Communications. He was the recipient of the First Prize in National Instruments ASEAN Virtual Instrumentation Applications Contest in 2007 and 2010, the Best Poster Award at the IEEE ANTS 2014, the IEEE Comsnets 2015 and 2016 conferences.

ANAND SRIVASTAVA received the M.Tech. and Ph.D. degrees from the Indian Institute of Technology Delhi, New Delhi, India. Before joining IIIT Delhi, he was the Dean and a Professor with the School of Computing and Electrical Engineering, Indian Institute of Technology Mandi, Mandi, India, and also an Adjunct Faculty with IIT Delhi. Prior to this, he was with Alcatel-Lucent-Bell Labs, India, as Solution Architect for access and core networks. Before joining Alcatel-Lucent, he had a long stint (20 years) with the Center for Development of Telematics (CDOT), a Telecom Research Center of Government of India, where he was the Director and a Member of the CDOT Board. During his stay in CDOT, he provided technical leadership and motivation to extremely qualified team of engineers engaged with the development of national level projects in the areas of telecom security systems, network management systems, intelligent networks, operations support systems, access networks (GPON), and optical technology-based products. Majority of these projects were completed successfully and commercially deployed with the public network. He was also closely involved with ITU-T, Geneva in Study Group 15 and represented India for various optical networking standards meetings. His research interests include optical core and access networks, vehicleto-vehicle communications, fiber-wireless (FiWi) architectures, optical signal processing, and visible light communications.

GOURAB GHATAK is currently an Assistant Professor with the Department of Electrical Engineering, Indian Institute of Technology Delhi, New Delhi, India, and the Ph.D. degree from the University of Paris-Saclay, France. During his doctoral studies, he was also employed with CEA-Grenoble, where he worked on the design and planning of multi-tier heterogeneous wireless networks with millimeter-wave small cells. Prior to that, he was a Visiting Research Scholar with TU Dresden, Dresden, Germany, where he developed preamble designs with low out-of-band radiation for channel estimation. He has authored or coauthored more than 40 journal and conference papers and is the inventor of five patents. His research interests include stochastic geometry, wireless communications, and machine learning for wireless networks.